Distributed Control of Islanded DC Microgrids: A Passivity-Based Game Theoretical Approach

Zao Fu, Carlo Cenedese, *Member, IEEE*, Michele Cucuzzella, *Member, IEEE*, Wenwu Yu, *Senior Member, IEEE*, and Jacquelien M. A. Scherpen, *Fellow, IEEE*

***Abstract*— In this article, we consider a dc microgrid composed of distributed generation units (DGUs) trading energy among each other, where the energy price depends on the total current generated by all the DGUs. We then use a Cournot aggregative game to describe the self-interested interaction among the DGUs, where each DGU aims at minimizing the deviation with respect to the given reference signals and maximizing the revenue from the sale of the generated power. Thus, we design a fully distributed continuous-time equilibrium-seeking algorithm to compute the generalized Nash equilibrium (GNE) of the game. We interconnect the designed decision-making algorithm with the dynamics of the microgrid in a passive way, and, by leveraging passivity theory, we prove the convergence of the closed-loop system trajectory to a feasible operating point that is also a Nash equilibrium of the collective aggregative game. Finally, we present extensive simulation results that validate the proposed distributed optimal control scheme, showing excellent performance.**

***Index Terms*— DC microgrids, distributed optimization, energy trading, game theory, passivity.**

Manuscript received 29 November 2023; revised 2 March 2024; accepted 20 May 2024. This work was supported in part by the National Science and Technology Major Project of China under Grant 2022ZD0120001, in part by the National Natural Science Foundation of China under Grant 62233004 and Grant 62073076, in part by the Jiangsu Provincial Scientific Research Center of Applied Mathematics under Grant BK20233002, in part by the China Scholarship Council under Grant 202006090138, in part by the Dutch Research Council (NWO) under Grant ESI.2019.005, and in part by the NCCR Automation, a National Centre of Competence in Research, funded by the Swiss National Science Foundation under Grant 180545. An earlier version of this article was presented at the 2022 IEEE 61st Conference on Decision and Control (CDC) [DOI: 10.1109/CDC51059.2022.9992327]. Recommended by Associate Editor N. Quijano. *(Corresponding authors: Michele Cucuzzella; Wenwu Yu.)*

Zao Fu is with the School of Cyber Science and Engineering, Southeast University, Nanjing 211189, China, and also with the Jan C. Willems Center for Systems and Control, ENTEG, Faculty of Science and Engineering, University of Groningen, 9747 AG Groningen, The Netherlands (e-mail: 230189383@seu.edu.cn).

Carlo Cenedese is with the Department of Information Technology and Electrical Engineering, ETH Zürich, 8002 CH Zürich, Switzerland (e-mail: ccenedese@ethz.ch).

Michele Cucuzzella is with the Department of Electrical, Computer and Biomedical Engineering, University of Pavia, 27100 Pavia, Italy, and also with the Jan C. Willems Center for Systems and Control, ENTEG, Faculty of Science and Engineering, University of Groningen, 9747 AG Groningen, The Netherlands (e-mail: michele.cucuzzella@unipv.it).

Wenwu Yu is with the School of Mathematics, Southeast University, Nanjing 211189, China (e-mail: wwyu@seu.edu.cn).

Jacquelien M. A. Scherpen is with the Jan C. Willems Center for Systems and Control, ENTEG, Faculty of Science and Engineering, University of Groningen, 9747 AG Groningen, The Netherlands (e-mail: j.m.a.scherpen@rug.nl).

Digital Object Identifier 10.1109/TCST.2024.3405711

NOMENCLATURE

I_i	Output current.
u_i	Voltage control input.
V_i	Load voltage.
R_i, L_i	Filter resistance, inductance.
C_i	Shunt capacitor.
$I_{L,i}$, $Z_{L,i}$	Load current, impedance.
$R_{l,k}$, $L_{l,k}$	Line resistance, inductance.
$I_{l,k}$	Line current.

I. INTRODUCTION

NOWADAYS, the increasing spread of energy communities, which influence and in turn are influenced by the energy trading market, gives rise to a complex networked power system requiring the design of a holistic control framework that encompasses both the physical and the decision-making systems. More precisely, a suitable control system should not only make the physical system operate safely and efficiently, but also embed economic-aware and cost-effective control policies [2]. In fact, the lack of a holistic approach may drive the overall system to a suboptimal operating point. On the other hand, developing such a holistic framework to control and optimize the whole system increases considerably the complexity of its design and analysis.

In this article, we consider a dc microgrid, whose dynamics are subject to physical and economic constraints that ensure its feasibility and economic operation [3]. For such a heterogeneous and possibly large-scale system, a centralized control scheme is not suitable since the required computational and communication resources would be prohibitive. This problem can be overcome by designing fully distributed control schemes [4]. Therefore, to increase the effectiveness of the energy dispatch in dc microgrids, it is of paramount importance to design an optimal distributed control scheme that incorporates the market trading mechanism.

A. Literature Overview

In the past decade, advanced control strategies have been designed to stabilize and optimize dc microgrids (see [5], [6], and the references therein). More precisely, to guarantee a proper and safe functioning of the devices connected to the microgrid, and prevent the overstressing of any source, the

main control goals in dc microgrids are voltage regulation and fair current sharing. To achieve these objectives, decentralized and distributed control schemes have been proposed in the literature (see [7], [8], [9], [10], [11], [12], [13], [14], [15], [16], and the references therein). In [17], [18], [19], [20], and [21], distributed optimal control algorithms have been proposed to achieve the aforementioned objectives and, at the same time, solve an optimization problem such as the minimization of the generation costs and power losses and/or the maximization of a utility function. In particular, the growing need to optimize power dispatch and active participation in the energy markets is attracting more and more researchers' attention toward the design of adequate decision-making systems.

Based on distributed optimization [22], the research on distributed decision-making systems can be roughly divided into two categories: discrete-time and continuous-time algorithms. Nedic et al. [23] and Liu et al. [24] propose discrete-time algorithms converging with a linear rate to the consensual minimizer. On the other hand, tools from nonsmooth analysis have been exploited in [25] and [26] to develop continuous-time algorithms converging to the consensual minimizer. Moreover, when the agents are noncooperative, then the decision-making process can be cast as a game. Also, in this case the literature is divided into two categories: discrete- and continuous-time algorithms. Using results from operator theory, several discrete-time distributed equilibrium-seeking algorithms have been proposed for aggregative games [27], [28], [29]. Similarly, continuous-time Nash equilibrium-seeking algorithms based on projection dynamics have been developed in [30], [31], [32], [33], and [34]. Bianchi and Grammatico [35, Sec. 6] propose a similar algorithm for heterogeneous multi-integrator dynamics, where the game is assumed unconstrained. These decision systems have been successfully applied to a plethora of applications such as tertiary control of power systems [6], charging of electric vehicles [36], [37], and Cournot market competition [29].

B. Article Contribution

In summary, research on both dc microgrid control and distributed decision-making systems is abundant. However, there is a lack of results that integrate both topics to develop a holistic framework. Our work aims at bridging this gap. More precisely, inspired by Cucuzzella et al. [20], we design a fully distributed continuous-time control scheme ensuring the stability and economically efficient operation of the microgrid.

The decision-making system is based on an energy trading market mechanism and is modeled as an aggregative game among all the distributed generation units (DGUs). To the best of our knowledge, this is the first work that uses passivity theory to interconnect a continuous-time fully distributed Nash equilibrium-seeking algorithm with the dynamics of a dc microgrid. The use of operator theory allows us to study the resulting interconnected closed-loop system and prove that the corresponding trajectory converges to a desired equilibrium for a suitable choice of the controller gains, for which explicit tuning rules are provided. Compared with [20], in this work, we include the energy trading mechanism, which leads to a collection of interdependent optimization problems, where the couplings arise in both the objective function and constraints. Moreover, differently from [20], we interconnect the dc microgrid and the decision-making system in such a way that the steady-state value of the interconnection port is equal to zero, thereby not altering the desired equilibrium point.

Compared with the preliminary results of this work that appeared in [1], the major advantages of this article rely on the following: 1) employing projection dynamics to satisfy local constraints; 2) using monotonicity to analyze the closed-loop convergence; and 3) interconnecting the microgrid and the decision system in a suitable way that does not affect the solution of the optimization problem.

C. Article Organization

In Section II, we introduce the microgrid model and its stability properties. In Section III, we formulate the problem and explain the control objectives. In Section IV, we analyze the problem formulated in Section III. In Section V, we design a distributed control strategy and discuss its convergence properties. We show and discuss simulation results in Section VI. Conclusions and directions for future works are gathered in Section VII. Finally, the reader can find in the Appendix the preliminaries on the projection operator and the proofs of all the results.

D. Notation and Preliminaries

1) Notation: $\mathbf{0}$, $\mathbf{1}$, $\mathbb{0}$, and $\boldsymbol{I}$ represent 0-vector, 1-vector, 0-matrix, and the identity matrix with appropriate dimensions, respectively. $\mathbb{R}^n$ denotes the n-dimensional Euclidean space, and $\mathbb{R}^n_+$ denotes the n-dimensional non-negative orthant. Given a vector $[x_1^\top, \dots, x_n^\top]^\top$, we compactly denote it by $\mathrm{col}(x_1, \dots, x_n)$ or $\mathrm{col}(x_i)_{i\in(1,\dots,n)}$. For convenience, we define $x_{-i} = \mathrm{col}(x_1, \dots x_{i-1}, x_{i+1}, \dots, x_n)$. The dimension of a vector x or the cardinality of a set $\mathcal{N}$ is denoted by $|x|$ and $|\mathcal{N}|$, respectively. $\mathrm{diag}(A_i)_{i\in(1,\dots,n)}$ denotes the matrix whose ith diagonal block is $A_i \in \mathbb{R}^{p\times q}$. The Cartesian product is denoted by $\prod$, and $\prod_{i=1}^n \Omega_i \triangleq \Omega_1 \times \cdots \times \Omega_n$. Note that, for the sake of clarity, most of the time, we denote diagonal matrices by D. $\{A\}_{i,j}$ represents the element that is located in the ith row and jth column of the matrix A. $\{x\}_i$ represents the ith element of the vector x. $A \succ 0$ ($\succeq 0$) means that A is symmetric positive (semi) definite. $\otimes$ denotes the Kronecker product, and $\circ$ denotes the Hadamard product. $\|x\|$ represents the Euclidean norm of x. $\|x\|_G$ denotes the G-norm of x, where G can be a positive definite or semidefinite matrix, and $\|x\|_G = \sqrt{x^\top G x}$. $\mathrm{span}(x)$ denotes the generating subspace of x. Let $\mathrm{bnd}(\Omega)$ and $\mathrm{int}(\Omega)$ represent the boundary and interior of the closed set Ω, respectively. $\mathrm{zer}(\mathcal{A})$ represents the set of zeros of the operator $\mathcal{A}$. Given a signal x, throughout this article we use the following notation.

1) $\hat{x}$ denotes the decision variable associated with x.
2) x^r denotes the reference value for x.
3) x^{ne} and x^* denote the generalized Nash equilibrium (GNE) and the equilibrium of x, respectively.

2) Preliminaries: The solution of a variational inequality VI(F, Ω) corresponds to a vector x satisfying

$$x \in \Omega, \quad \langle y - x, F(x) \rangle \geq 0 \quad \forall y \in \Omega \tag{1}$$

where $\Omega \in \mathbb{R}^n$ and $F : \Omega \rightrightarrows \mathbb{R}^n$ is a set-value map. For convenience, we use SOL(F, Ω) to represent the solution of the VI(F, Ω). Moreover, $\mathcal{N}_\Omega(x)$ denotes the normal cone of the set Ω at $x \in \Omega$, and $\mathcal{N}_\Omega(x) = \{z \mid z^\top (x-y) \leq 0, \forall y \in \Omega\}$. According to [38, eq. (1.1.3)], it follows that $x \in \Omega$ solves the VI(F, Ω) if and only if it satisfies $F(x) \in -\mathcal{N}_\Omega(x)$. The notation $\mathcal{P}_\Omega$ denotes the projection operator on the set Ω, and $\mathcal{P}_\Omega(x) = \arg\min_{y \in \Omega} \|x - y\|$. The function $\mathcal{T}_\Omega(x, F(x))$ is equivalent to projecting the vector $F(x)$ onto the tangent cone of Ω at x, i.e.,

$$\mathcal{T}_\Omega(x, F(x)) = \lim_{\xi \to 0} \frac{\mathcal{P}_\Omega(x + \xi F(x)) - x}{\xi}. \tag{2}$$

Additional preliminaries on the projection operator are reported in Appendix A.

II. DC Microgrid Model

In this section, we introduce the microgrid dynamics and its properties. Following [12] and the references therein, we consider an islanded dc microgrid consisting of n DGUs, each of which supplies a "ZI" load, where "Z" and "I" represent the constant impedance and current components of the load, respectively. The DGUs are interconnected through m transmission lines. We use the index sets $\mathcal{N} \triangleq \{1, \dots, n\}$ and $\mathcal{E} \triangleq \{1, \dots, m\}$ for the DGUs and the transmission lines, respectively. We assume that each DGU is responsible for satisfying the physical constraints of one or more transmission lines connected to it [39], [40]. Yet, each transmission line is managed by only one DGU.[1] We use $\mathcal{E}_i \subseteq \mathcal{E}$ to represent the index set containing all the transmission lines managed by the DGU $i \in \mathcal{N}$. Therefore, $\mathcal{E}_1, \dots, \mathcal{E}_n$ represent a partition of $\mathcal{E}$ satisfying

$$\bigcap_{i \in \mathcal{N}} \mathcal{E}_i = \emptyset, \quad \bigcup_{i \in \mathcal{N}} \mathcal{E}_i = \mathcal{E}. \tag{3}$$

Fig. 1 depicts the equivalent circuit of the DGU $i \in \mathcal{N}$ and transmission line $k \in \mathcal{E}_i \subseteq \mathcal{E}$; see also Nomenclature for the explanation of the physical meaning of the used symbols. We model the interconnections among the DGUs as a (arbitrary oriented) connected undirected graph $\mathcal{G}(\mathcal{N}, \mathcal{E})$.

Then, based on the Kirchhoff laws, the dynamics of the considered dc microgrid are as follows:

$$L\dot{I} = -V - RI + u \tag{4a}$$
$$C\dot{V} = I + BI_l - Z_L^{-1} V - I_L \tag{4b}$$
$$L_l \dot{I}_l = -R_l I_l - B^\top V \tag{4c}$$

where L, C, R, $Z_L \in \mathbb{R}^{n \times n}$ and L_l, $R_l \in \mathbb{R}^{m \times m}$ are diagonal positive definite matrices, e.g., $L \triangleq \text{diag}(L_i)_{i \in \mathcal{N}}$. Moreover, $u, I, V \in \mathbb{R}^n$ and $I_l \in \mathbb{R}^m$ denote, respectively, the vectors collecting all the nodes and edges components, e.g., $u \triangleq \text{col}(u_1, \dots, u_n)$. Moreover, $B \in \mathbb{R}^{n \times m}$ is the incidence matrix

[1]Providing a systematic procedure to select the partition of the transmission lines is out of the scope of this article and left as a future work.

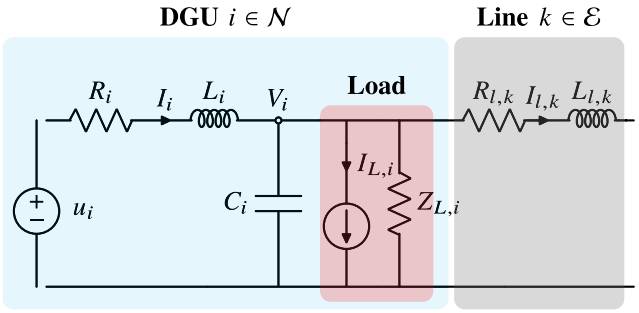

Fig. 1. Electrical scheme of the DGU $i \in \mathcal{N}$ and the transmission line $k \in \mathcal{E}$.

associated with $\mathcal{G}(\mathcal{N}, \mathcal{E})$. We refer the interested reader to [12] for further model details. Now, for convenience, we define $x_i \triangleq \text{col}(I_i, V_i, I_{c,i}) \in \mathbb{R}^{2+|\mathcal{E}_i|}$ to represent the state vector of the DGU $i \in \mathcal{N}$, where $I_{c,i} \triangleq \text{col}(I_{l,k})_{k \in \mathcal{E}_i} \in \mathbb{R}^{|\mathcal{E}_i|}$. Moreover, let $x \triangleq \text{col}(x_i)_{i \in \mathcal{N}}$. Then, the dynamics in (4) can be rewritten compactly as follows:

$$\boldsymbol{D}_x \dot{x} = Hx + Qu + d \tag{5}$$

where $\boldsymbol{D}_x$, H, and Q are matrices appropriately defined, $d_i = \text{col}(0, I_{L,i}, \mathbf{0})$, and $d \triangleq \text{col}(d_i)_{i \in \mathcal{N}}$. More precisely, $\boldsymbol{D}_x \succ 0$ is diagonal and H can be shown to be full rank. In the following lemma we recall from [11, Proposition 5] that (5) is shifted passive, see [41, Definition 2] for the definition of shifted passivity.

Lemma 1 (Shifted Passivity of (5)): The dynamical system (5) is shifted passive with supply rate $(u - u^*)^\top (I - I^*)$ and storage function

$$E(x) = \frac{1}{2} \|x - x^*\|_{\boldsymbol{D}_x}. \tag{6}$$

Proof: The proof is reported in Appendix B.

III. Problem Formulation

In this section, we design a Cournot aggregative game [42, Definition 1], which has as Nash equilibrium a desired (safe and optimal) operating point of the microgrid dynamics (5). Specifically, every DGU $i \in \mathcal{N}$ has to satisfy the following local constraints:

$$V_i + R_i I_i - u_i = 0 \tag{7a}$$
$$V_i^{\min} \leq V_i \leq V_i^{\max} \tag{7b}$$
$$I_{c,i}^{\min} \leq I_{c,i} \leq I_{c,i}^{\max} \tag{7c}$$

where (7a) comes from (4a) in steady state, and the superscripts "min" and "max" in (7b) and (7c) denote the minimum and maximum allowed values for the corresponding variable, respectively. Therefore, the local feasible region is defined as follows:

$$\Omega_i \triangleq \left\{ (u_i, x_i) \in \mathbb{R}^{3+|\mathcal{E}_i|} \mid (7) \text{ is satisfied} \right\}. \tag{8}$$

To guarantee feasible steady-state operating conditions of the microgrid, the following set of coupling constraints also needs to be satisfied:

$$K \triangleq \left\{ (u, x) \in \mathbb{R}^{m+3n} \;\middle|\; \begin{array}{c} I + BI_l - Z_L^{-1} V = I_L \\ R_l I_l + B^\top V = \mathbf{0} \\ -I_l^\top B^\top V^r \leq P_{\text{loss}}^{\max} \end{array} \right\} \tag{9}$$

where the first two equality constraints come from (4b) and (4c) in the steady state. Also, the term $I_l^\top B^\top V^r$ in (9) represents an approximation[2] of the steady-state total power loss in the transmission lines, and $P_{\text{loss}}^{\max} > 0$ denotes the corresponding upper bound. Note that $\text{col}(I_{c,i})_{i\in\mathcal{N}}$ is effectively a permutation of I_l used to ease the notation.

Now, for the sake of simplicity, we rewrite the set (9) in the following compact form:

$$K = \left\{(u, x) \in \mathbb{R}^{m+3n} \mid Ax - b \leq \mathbf{0}\right\} \tag{10}$$

where $A \in \mathbb{R}^{(2m+2n+1)\times(m+2n)}$ and $b \in \mathbb{R}^{2m+2n+1}$ are appropriately defined to rearrange the order of the constraints in (9). Moreover, A in (10) is composed of n blocks, i.e., $A = [A_1, \ldots, A_n]$, with $A_i \in \mathbb{R}^{(2m+2n+1)\times(2+|\mathcal{E}_i|)}$ for all $i \in \mathcal{N}$. Consequently, $Ax \leq b$ can be written as follows:

$$\sum_{i=1}^{n} A_i x_i - b_i \leq \mathbf{0}$$

where $b_i \in \mathbb{R}^{2m+2n+1}$ for all $i \in \mathcal{N}$. Therefore, the feasible decision set of each DGU $i \in \mathcal{N}$ reads as

$$\pi_i\left(x_{-i}\right) = \left\{ (u_i, x_i) \in \Omega_i \mid A_i x_i - b_i + \sum_{j\neq i} A_j x_j - b_j \leq 0 \right\}$$

while the collective feasible set is $K_\Omega \triangleq K \cap \Omega$, where $\Omega = \prod_{i\in\mathcal{N}} \Omega_i$. We can now introduce the main goal of this article, which can be formulated as an aggregative game problem, i.e.,

$$\forall\, i \in \mathcal{N}, \quad \begin{cases} \min\limits_{u_i, x_i} \; f_i\left(u_i, x_i, \sigma_I\right) \\ \text{s.t. } (u_i, x_i) \in \pi_i\left(x_{-i}\right) \end{cases} \tag{11}$$

with

$$f_i\left(u_i, x_i, \sigma_I\right) = f_{1,i}\left(x_i, u_i\right) - f_{2,i}\left(x_i, \sigma_I\right) \tag{12a}$$

$$f_{1,i}\left(u_i, x_i\right) \triangleq \frac{\alpha_{u_i}}{2}(u_i - u_i^r)^2 + \frac{1}{2}\|x_i - x_i^r\|_{W_i}^2 \tag{12b}$$

$$f_{2,i}\left(x_i, \sigma_I\right) \triangleq \left(\bar{p} - p_r\sigma_I\right) V_i^r I_i \tag{12c}$$

where $\sigma_I \triangleq \sum_{i=1}^n I_i$ is the aggregative variable representing the total current generated by all the DGUs in the microgrid. The function $f_{1,i}(u_i, x_i)$ represents the cost associated with the input and state deviation of the DGU $i \in \mathcal{N}$ with respect to the corresponding references, $\alpha_{u_i} \in \mathbb{R}_+$, and the constant matrix $W_i \triangleq \text{diag}(\alpha_{I_i}, \alpha_{V_i}, \text{diag}(\alpha_{I_{l,k}})_{k\in\mathcal{E}_i}) \succ 0$ is tuning parameters. On the other hand, $f_{2,i}(x_i, \sigma_I)$ is a concave function based on the Cournot model (see [43], [44], [45]) and represents an approximation[1] of the profit obtained by DGU $i \in \mathcal{N}$ from selling the (approximated) generated power $V_i^r I_i$ at the price $(\bar{p} - p_r\sigma_I)$, with $\bar{p}, p_r \in \mathbb{R}_+$. The constant parameters u_i^r, x_i^r, α_{u_i}, and W_i are associated with the nominal set points and desired performance of the DGU $i \in \mathcal{N}$. In such a setting, each DGU can be considered a player in a game describing the energy trading among the DGUs. The trading price $(\bar{p} - p_r\sigma_I)$ is an aggregative quantity involving all the DGUs' decision states.

[2]The approximation comes from considering the voltage V to be equal to its reference value V^r. Since the proposed control scheme aims to regulate the microgrid voltage toward its desired reference [see (11) and (12b)], this is a reasonable approximation.

Remark 1: In practice, based on the specific energy market, the value of $\bar{p}$ in (12c) is chosen as the maximum energy price, while p_r is chosen depending on how quickly the price of energy changes in response to variations of the total generation σ_I (see [46] for more details). Since the quantity $(\bar{p} - p_r\sigma_I)$ can become negative for large values of σ_I, which would be unreasonable in practice, then, by inspecting the equality constraints in (9), the following assumption guarantees that the energy price is positive for all the feasible choices of σ_I and I.

Assumption 1 (Positive Cournot Price): Let the following inequality

$$\sum_{i=1}^{n}\left(\frac{V_i^{\max}}{Z_{L,i}} + I_{L,i}\right) < \frac{\bar{p}}{p_r} \tag{13}$$

hold for all $i \in \mathcal{N}$, i.e., $\bar{p} - p_r\sigma_I > 0$ for all $x \in \Omega$.

IV. Problem Analysis

This section derives the Karush–Kuhn–Tucker (KKT) conditions for the problem (11), which will be used in Section V to design the distributed decision-making system. First, to ensure the solvability of (11), we introduce the following assumption, which is common in the literature (see [38], [47]).

Assumption 2 (Nonempty Feasible Set): The collective feasible set is nonempty, i.e., $K_\Omega \neq \emptyset$.

The above assumption directly implies that $\pi_i(x_{-i})$ satisfies the Slater constraint qualification (SCQ) [38, Sec. 3.2] for all $i \in \mathcal{N}$ and $(u, x) \in K_\Omega$. Now, let the collective strategy $(u^{\text{ne}}, x^{\text{ne}})$ denote the GNE of (11), which is defined as follows (see [48, Sec. 5.2.3]).

Definition 1 (GNE): The couple $(u^{\text{ne}}, x^{\text{ne}}) \in K_\Omega$ is a GNE of (11) if and only if the following inequality holds for all $i \in \mathcal{N}$:

$$f_i\left(u_i^{\text{ne}}, x_i^{\text{ne}}, \sigma_I^{\text{ne}}\right) \leq f_i\left(u_i, x_i, \bar{\sigma}_i\right) \quad \forall\,(u_i, x_i) \in \pi_i\left(x_{-i}^{\text{ne}}\right) \tag{14}$$

where $\bar{\sigma}_i = I_i + \sum_{j\neq i} I_j^{\text{ne}}$.

Note that Assumption 2 also implies that the duality gap is equal to zero [48, Sec. 5.2.3]. According to [49, Sec. 2], the GNE $(u^{\text{ne}}, x^{\text{ne}})$ of the problem (11) and its dual solution $\lambda^{\text{ne}} \in \mathbb{R}_+^{2m+2n+1}$ are the solution to the following set of inclusions:

$$\forall i \in \mathcal{N}, \quad \begin{cases} -F_i(u_i, x_i, \sigma_I) - \tilde{A}_i^\top \lambda_i \in \mathcal{N}_{\Omega_i}(u_i, x_i) \\ \sum\limits_{i=1}^{n} A_i x_i - b_i \in \mathcal{N}_{\mathbb{R}_+^{2m+2n+1}}(\lambda_i) \end{cases} \tag{15}$$

where $\tilde{A}_i \triangleq [\mathbf{0}, A_i]$, and

$$F_i\left(u_i, x_i, \sigma_I\right) = \begin{bmatrix} \nabla_{u_i} f_i\left(u_i, x_i, \sigma_I\right) \\ \nabla_{x_i} f_i\left(u_i, x_i, \sigma_I\right) \end{bmatrix} \tag{16}$$

represents the pseudo gradient associated with the objective function (12a) of the DGU $i \in \mathcal{N}$. Now, note that the solution to (15) is not unique, and in turns the GNE of (11) may also be not unique [49, Sec. 3]. Then, to make the problem tractable, we focus on a subset of GNEs, called normalized Nash equilibrium (NNE) [49, Definition 3.2], which can be characterized as the solution set of a VI. Since the feasible

set K_Ω is a polyhedron, the NNE of (11) can be sought in a distributed way (see [50]). For the reader's convenience, we introduce now the definition of NNE.

Definition 2 (NNE): A GNE $(u^{\mathrm{ne}}, x^{\mathrm{ne}}) \in K_\Omega$ is an NNE associated with $r \in \mathbb{R}^n_+$ if and only if the triplet $(u^{\mathrm{ne}}, x^{\mathrm{ne}}, \lambda^{\mathrm{ne}})$ satisfies (15) and the following condition

$$r_1 \lambda_1^{\mathrm{ne}} = \cdots = r_n \lambda_n^{\mathrm{ne}}. \tag{17}$$

According to [49, Proposition 3.2], any NNE $(u^{\mathrm{ne}}, x^{\mathrm{ne}}) \in K_\Omega$ associated with $r \in \mathbb{R}^n_+$ can be cast as a solution of the VI(F_r, K_Ω), where $F_r \triangleq \mathrm{col}(r_i F_i)_{i\in\mathcal{N}}$. From [38, Th. 2.3.3], it follows that the NNE is unique if and only if F_r is strongly monotone. As shown in the following lemma, we can ensure that F_r is strongly monotone by suitably tuning the (controller) parameter α_{I_i} for all $i \in \mathcal{N}$, appearing in W_i in (12b).

Lemma 2 (Strong Monotonicity): For a given $r \in \mathbb{R}^n_+$, if α_I satisfies

$$\alpha_{I_i} + \left(\frac{(6-n)\, p_r V_i^r}{2} - \frac{1}{2r_i} \sum_{j=1}^{n} r_j\, p_r V_j^r \right) > 0 \quad \forall i \in \mathcal{N} \tag{18}$$

then F_r is strongly monotone on K_Ω.

Proof: The proof is reported in Appendix C.

Let $\mathcal{G}_{\mathrm{c}}(\mathcal{N}, \mathcal{E}_{\mathrm{c}})$ denote the graph associated with the communication network among the DGUs. For the sake of simplicity in the exposition and without loss of generality, we assume hereafter that the communication graph is the same as $\mathcal{G}(\mathcal{N}, \mathcal{E})$, while in general $\mathcal{E}$ and $\mathcal{E}_{\mathrm{c}}$ can be different, provided that $\mathcal{G}_{\mathrm{c}}$ satisfies the following assumption.

Assumption 3 (Graph): The graph $\mathcal{G}_{\mathrm{c}}(\mathcal{N}, \mathcal{E}_{\mathrm{c}})$ is undirected and connected.

Under Assumption 3, the Laplacian matrix L_{c} associated with the communication graph $\mathcal{G}_{\mathrm{c}}$ is positive semidefinite. For convenience, we define $\boldsymbol{L}_{\mathrm{c}} \triangleq L_{\mathrm{c}} \otimes \boldsymbol{I}$ to denote the extended Laplacian matrix with suitable dimensions. Next, following steps similar to those in [50], we endow the KKT conditions in (15) with an auxiliary variable θ_i for each DGU $i \in \mathcal{N}$, and use all of them to force the dual variables $\lambda_1, \ldots, \lambda_n$ to reach the weighted consensus (17) at the equilibrium. Then, we can obtain the following optimal conditions:

$$F_r\,(u, x, \sigma_I \mathbf{1}) + \tilde{\boldsymbol{A}}^{\top} \boldsymbol{D}_r \lambda \in -\mathcal{N}_\Omega\,(u, x) \tag{19a}$$

$$\boldsymbol{D}_r \left(\boldsymbol{L}_{\mathrm{c}} \boldsymbol{D}_r \lambda + \boldsymbol{L}_{\mathrm{c}} \theta - \boldsymbol{A} x + \boldsymbol{b} \right) \in -\mathcal{N}_{\mathbb{R}^{n(2m+2n+1)}_+}(\lambda) \tag{19b}$$

$$-\boldsymbol{L}_{\mathrm{c}} \boldsymbol{D}_r \lambda = \mathbf{0} \tag{19c}$$

where $\tilde{\boldsymbol{A}} = \mathrm{diag}(\tilde{A}_i)_{i\in\mathcal{N}}$, $\boldsymbol{A} = \mathrm{diag}(A_i)_{i\in\mathcal{N}}$, $\boldsymbol{b} = \mathrm{col}(b_i)_{i\in\mathcal{N}}$, and $\boldsymbol{D}_r \triangleq \mathrm{diag}(r_i \boldsymbol{I})_{i\in\mathcal{N}}$. Note that we can rewrite the KKT conditions associated with the decision system (19) in the following compact form:

$$G_r\,(z) \in -\mathcal{N}_U\,(z) \tag{20}$$

where $U \triangleq \Omega \times \mathbb{R}^{n(2m+2n+1)}_+ \times \mathbf{0}$, G_r denotes the map on the left-hand side of (19), and $z \triangleq \mathrm{col}(u, x, \lambda, \theta)$. The next lemma ensures that a solution of (19) is an NNE satisfying (17).

Lemma 3 (Uniqueness): If Assumptions 2 and 3 and (18) hold, then the following statements are equivalent.

1) The GNE $(u^{\mathrm{ne}}, x^{\mathrm{ne}})$ is the unique NNE of (11) associated with $r \in \mathbb{R}^n_+$.
2) There exist $\lambda^{\mathrm{ne}} \in \mathbb{R}^{n(2m+2n+1)}_+$ and $\theta^{\mathrm{ne}} \in \mathbb{R}^{n(2m+2n+1)}$ such that the quadruple $z^{\mathrm{ne}} = (u^{\mathrm{ne}}, x^{\mathrm{ne}}, \lambda^{\mathrm{ne}}, \theta^{\mathrm{ne}})$ solves (19).
3) $z^{\mathrm{ne}} \in \mathrm{zer}(G_r + \mathcal{N}_U)$, i.e., $z^{\mathrm{ne}} \in \mathrm{SOL}(G_r, U)$.

Proof: The proof follows similar steps to the ones in [50, Th. 2] adapted to a setup akin to [28, Lemma 1].

Based on the results of Lemma 3, we can rely on the well-established field of zero-finding algorithms to compute an NNE of the original game (11) (see [51, Sec. 2]).

Remark 2: Since $\boldsymbol{D}_r \boldsymbol{L}_{\mathrm{c}}$ is not full rank, then a feasible point satisfying (17) does not meet the strict Mangasarian–Fromovitz constraint qualification [38, Sec. 3.2]. Consequently, the dual solution θ^{ne} is not unique [38, Proposition 3.2.1]. If $V^r \notin \mathrm{span}(\mathbf{1}_n)$, and thus all the rows of A are linearly independent [see the inequality (9)], then we can deduce that the linear independence constraint qualification holds for all $(u, x) \in K_\Omega$ and thus $(u^{\mathrm{ne}}, x^{\mathrm{ne}}, \lambda^{\mathrm{ne}})$ satisfying (19) is unique.

V. Controller Design and Convergence Analysis

In this section, we first design a distributed decision system for the microgrid and then interconnect it with the microgrid dynamics in a passive way. Based on passivity, projection dynamics, and Lyapunov theory, we then analyze the convergence of the resulting interconnected system.

A. Feedback Interconnection and Estimation of σ_I

1) Interconnection of the Physical and Decision System: The decision system we propose is composed of two subsystems. One is used to seek a solution solving (19), while the other estimates in a distributed manner the aggregative quantity σ_I appearing in the objective function of each DGU $i \in \mathcal{N}$, viz. (12c). Note that in the following we denote by $\hat{x}$ the decision variables (primal variables) associated with the state of the corresponding microgrid dynamics (5).

Now, using Lemma 2 and the steps akin to those in [29, Sec. 3.2], we can characterize the monotonicity properties of G_r in (20).

Proposition 1 (Monotonicity of G_r): If Assumptions 2 and 3 and (18) hold, then G_r in (20) is (maximal) monotone in U.

Proof: The proof is reported in Appendix D.

Furthermore, from Lemma 3 and [38, Th. 2.3.5], it follows that the solution set of (20) is convex and compact. These two features will be the keystone for the development of our algorithm. Starting from (20), we design the following projection dynamics converging to a solution of the VI(G_r, U), i.e.,

$$\dot{\hat{z}} = \mathcal{T}_U\left(\hat{z}, -G_r\left(\hat{z}\right) - \epsilon \Delta_{\hat{z}} e_I\right), \quad e_I \triangleq I - \hat{I} \tag{21}$$

where $\epsilon > 0$ is a suitable feedback gain, $\hat{z} \triangleq \mathrm{col}(u, \hat{x}, \lambda, \theta)$, and the diagonal matrix $\Delta_\star$ is a constant matrix defined as $\{\Delta_\star\}_{ii} = 1$, if $\{\nabla_u(\star)\}_i = 1$, and $\{\Delta_\star\}_{ii} = 0$, otherwise. The number of rows of $\Delta_\star$ coincides with the dimension of the associated subscript $\star$, e.g., in (21) $\Delta_{\hat{z}}$ has as many rows as

the dimension of $\hat{z}$, while the number of columns coincides with the dimension of e_I. Note that $\Delta_\star$ is used to make the error e_I affect only the dynamics of u.

2) Local Estimation of the Aggregate Quantity: In practice, the aggregative quantity σ_I in $G_r(\hat{z})$ depends on the global information, thus it prevents the implementation of a fully distributed algorithm. To overcome such a problem, we design a distributed estimator converging asymptotically to the actual value of σ_I. Next, we introduce such a distributed system with the state variables $\eta, \nu \in \mathbb{R}^n$, i.e.,

$$\begin{aligned} \dot{\eta} &= -\eta - L_c\eta - L_c\nu + n\hat{I} \\ \dot{\nu} &= L_c\eta. \end{aligned} \tag{22}$$

For each DGU $i \in \mathcal{N}$, η_i represents the local estimation of σ_I while the auxiliary variable ν_i is used to reach consensus among all the other estimations. Next, we analyze the steady-state properties of (22). Letting $\dot{\eta} = \dot{\nu} = \mathbf{0}$, it follows, for all $i \in \mathcal{N}$, that

$$L_c\eta = \mathbf{0}, \quad \mathbf{1}^\top(\eta + L_c\nu - n\hat{I}) = 0, \ \ \eta_i = \sum_{i=1}^{n} \hat{I}_i. \tag{23}$$

Exploiting (23), we are now ready to complete the design of the distributed decision system and interconnect it with the physical system (5). Let $q_i \triangleq \mathrm{col}(u_i, \hat{x}_i)$ and $q = \mathrm{col}(q_i)_{i\in\mathcal{N}}$, then the closed-loop dynamics read as follows:

$$\boldsymbol{D}_x\dot{x} = Hx + Qu + d \tag{24a}$$
$$\varepsilon\dot{\eta} = -\eta - L_c\eta - L_c\nu + n\hat{I} \tag{24b}$$
$$\varepsilon\dot{\nu} = L_c\eta \tag{24c}$$
$$\kappa\dot{q} = \mathcal{T}_\Omega(q, -F_r(q,\eta) - \tilde{\boldsymbol{A}}^\top \boldsymbol{D}_r\lambda - \epsilon\Delta_q e_I) \tag{24d}$$
$$\kappa\dot{\lambda} = \mathcal{T}_{\mathbb{R}^{2m+2n+1}_+}\left(\lambda, \boldsymbol{D}_r\left(\boldsymbol{A}\hat{x} - b - \boldsymbol{L}_c\boldsymbol{D}_r\lambda - \boldsymbol{L}_c\theta\right)\right) \tag{24e}$$
$$\kappa\dot{\theta} = \boldsymbol{L}_c\boldsymbol{D}_r\lambda \tag{24f}$$

where the constants $\varepsilon > 0$ and $\kappa > 0$ are tuning parameters. The function $F_r(q,\eta)$ corresponds to the pseudo gradient (16), where the aggregative quantity σ_I, appearing in the gradient of each objective function $f_i(q_i, \sigma_I)$, is replaced by its local estimation η_i for all $i \in \mathcal{N}$. Hence, it follows that $F_r(q,\eta) = \mathrm{col}(r_i F_i(q_i, \eta_i))_{i\in\mathcal{N}}$, where

$$F_i(q_i, \eta_i) = \nabla_{q_i} f_{1,i}(q_i) + \begin{bmatrix} 0 \\ (p_r\eta_i + p_r\hat{I}_i - \bar{p})V_i^r \\ \mathbf{0} \end{bmatrix}.$$

Note that the interconnected system (24) is composed of three subsystems. Specifically, the subsystem (24a) represents the microgrid dynamics. The subsystem (24b) and (24c) represents the distributed estimation scheme of σ_I. Finally, the subsystem (24d)–(24f) represents the decision system, where (24d) are the dynamics of the primal variables, (24e) are the dynamics of the dual variables, and (24f) is used to achieve the weighted consensus (17). The interconnection between these three subsystems is depicted in Fig. 2, which also shows that each agent communicates only with its neighbors, and the topology of the communication network is described by the Laplacian matrix L_c. Thus, the proposed framework (24) is fully distributed. Moreover, (24d)–(24f) arise directly from the dynamics (21) and, together with (24b) and (24c), compose the fully distributed control system dynamics whose role is to compute the control input u for the system (24a), from which it receives $\Delta_q e_I$ as feedback (see [20]).

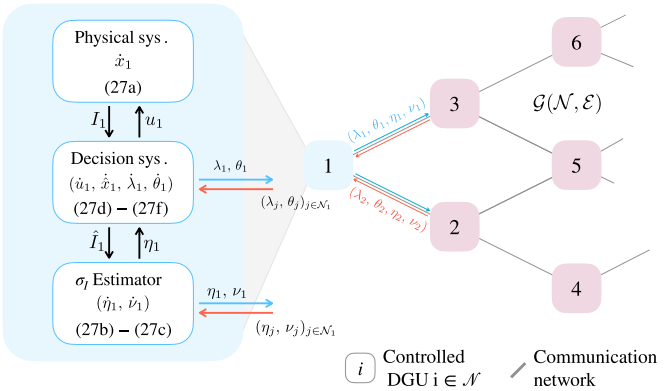

Fig. 2. Graphical representation of the interconnections among the subsystems in (24).

Remark 3: Calculating the value of a projection function is generally difficult, especially for continuous-time dynamical systems [52]. However, in our case, the projections in (24b)–(24f) are on the positive quadrant or on a low-dimensional hyperplane, which makes the computation easier.

Remark 4: The decision system can be implemented as a circuit system [53] and interconnected in parallel with the DGUs. In such a scenario, the decision system becomes robust with respect to the load changes. In other words, once the load changes, the decision system can steer the DGUs to a new equilibrium without changing any system parameter. As the number of the DGUs and transmission lines increases, the dimension of the decision system of each DGU also increases. Therefore, for a large-scale microgrid, it might be convenient to divide the whole network into smaller clusters containing a reasonable number of DGUs and transmission lines such that the dimension of the decision system does not become too large. Then, each cluster cooperates with the others in a higher level than that of the DGUs.

B. Deviation and Convergence Analysis

Let us denote the collective state of the decision system by $s \triangleq \mathrm{col}(\eta, \nu, q, \lambda, \theta)$ and $U_{\mathrm{ds}} \triangleq \mathbb{R}^{2n} \times U$. Then, similar to (21), we can compactly rewrite the dynamics (24b)–(24f) as follows:

$$\boldsymbol{D}_s\dot{s} = \mathcal{T}_{U_{\mathrm{ds}}}(s, -G_{\mathrm{ds}}(s) - \epsilon\Delta_s e_I) \tag{25}$$

where $\boldsymbol{D}_s \triangleq \mathrm{diag}(\varepsilon\boldsymbol{I}, \kappa\boldsymbol{I})$ and G_{ds} can be easily attained by the inspection of (24b)–(24f). The following proposition characterizes the uniqueness of the equilibrium of (24) and also shows that $x^* = \hat{x}^*$.

Proposition 2 (Unique Equilibrium): Let Assumptions 2 and 3 and (18) hold. Moreover, let (x^*, s^*) be an equilibrium of (24). Then, the following statements hold.

1) x^* and q^* are unique and satisfy $u^* = u^{\mathrm{ne}}$ and $x^* = \hat{x}^* = \hat{x}^{\mathrm{ne}}$. If $V^r \notin \mathrm{span}(\mathbf{1}_n)$, λ^* is also unique and satisfies $\lambda^* = \lambda^{\mathrm{ne}}$.

2) $s^* \in \mathrm{SOL}(G_{\mathrm{ds}}, U_{\mathrm{ds}})$.

Proof: The proof is reported in Appendix E.

Now, assuming that the trajectory of (24) converges to $s^* \in \mathrm{SOL}(G_{\mathrm{ds}}, U_{\mathrm{ds}})$, which will be proved in Theorem 2, we introduce a corollary that elaborates on the results of Proposition 2.

Corollary 1 (Equilibrium Equivalence): Let the assumptions of Proposition 2 hold. If the trajectory of (24) converges to $s^* \in \mathrm{SOL}(G_{\mathrm{ds}}, U_{\mathrm{ds}})$, given the initial condition $\theta(t_0)$, then θ^* is unique.

Proof: The proof is reported in Appendix F.

The following proposition introduces a condition for tuning the controller parameters.

Proposition 3 (Monotonicity Condition): If the condition

$$\forall\, i \in \mathcal{N}, \quad \begin{cases} 4\sqrt{c\left(r_i\alpha_{I_i} + r_i\, p_r\, V_i^r\right)} > \left|\dfrac{n\kappa - r_i\, p_r\, V_i^r\, \varepsilon}{\sqrt{\varepsilon\kappa}}\right| \\ 2\sqrt{r_i^2\alpha_{u_i}\,(1-c)\left(\alpha_{I_i} + p_r V_i^r\right)} > \epsilon \end{cases} \tag{26}$$

holds, where $0 < c < 1$, the function $\boldsymbol{D}_s^{-1}(G_{\mathrm{ds}}(s) + \epsilon\Delta_s e_I)$ is monotone with respect to s.

Proof: The proof is reported in Appendix G.

Remark 5: The controller in (24) is fully distributed. However, according to (26), the tuning of its parameters has to be done in a centralized way (once and offline). This is due to the fact that, for notation simplicity, we have preferred to choose ε, κ, and ϵ as scalars. Nevertheless, the tuning procedure can be made distributed by choosing different ε_i, κ_i, and ϵ_i for each DGU $i \in \mathcal{N}$, and paying attention to preserve the monotonicity of $\boldsymbol{D}_s^{-1}(G_{\mathrm{ds}}(s) + \boldsymbol{\epsilon}\Delta_s e_I)$, where $\boldsymbol{\epsilon} = \mathrm{diag}(\epsilon_i)_{i\in\mathcal{N}}$. Such distributed conditions can be derived from Appendix G; however, it is outside of the scope of this article. Moreover, (26) is associated only with the parameters of the DGU $i \in \mathcal{N}$ and $0 < c_i < 1$.

It is worth noting that (26) is only a sufficient condition for (41) in Appendix G. Moreover, different settings of ε and κ may cause a time separation between the subsystems in (24), and (24) can be considered as a singular perturbation system [54, Sec. 11]. Nevertheless, in this work, by virtue of the monotonicity of $\boldsymbol{D}_s^{-1}(G_{\mathrm{ds}}(s) + \boldsymbol{\epsilon}\Delta_s e_I)$, we do not need to invoke singular perturbation theory to analyze the stability of (24).

In the following two theorems, we present the major results of this article. Specifically, Theorem 1 establishes the convergence of s to s^*, and the passivity property of (25) with input $\epsilon\Delta_s e_I$.

Theorem 1 (Passivity and Convergence of (25)): Let Assumptions 2 and 3 hold. Given (25) and the storage function $W(s) = \frac{1}{2}\|s - s^*\|^2$, if $\varepsilon, \kappa, \epsilon > 0$ satisfy the condition (26), and $s(t_0) \in U_{\mathrm{ds}}$, then it follows that $s(t) \in U_{\mathrm{ds}}$ for all $t \geq t_0$ and the system (25) is shifted passive with respect to $W(s)$ and supply rate $-(\epsilon/\kappa)(u - u^*)^\top(I - I^*)$.

Proof: The proof is reported in Appendix H.

Note that setting $\epsilon = 0$ in (24d) implies that (24) becomes an open-loop system. In such a case, the decision system (24d)–(24f) does not receive any feedback from the physical system (24a), thus losing robustness. Moreover, it is in general desired to select a relatively small κ to endow the trajectory of the controller dynamics with a faster convergence. However, the condition (26) in Proposition 3 shows that selecting a larger ϵ shrinks the feasible range for κ and ε, which may increase the convergence rate of the trajectory of the dynamics (24).

TABLE I
PARAMETERS FOR EACH DGU

DGU	r_i	α_{I_i}	α_{V_i}	α_{u_i}	$\alpha_{I_{l,k}}$
1	1.06	10.6	0.75	1.1	1.4
2	1.03	10.1	0.62	1.4	1.9
3	1.05	10.2	0.85	1.8	1.7
4	1.04	10.5	0.93	1.1	1.9

Now, by exploiting the passive interconnection of the physical and decision system, the next theorem establishes that the trajectory of (24) converges to (x^*, s^*).

Theorem 2 (Convergence of (24)): Let Assumptions 2 and 3 and (18) hold, and let $\varepsilon, \kappa, \epsilon > 0$ satisfy the condition (26). Then, the trajectory of (24) converges to the desired equilibrium (x^*, s^*) satisfying $x^* = \hat{x}^* = \hat{x}^{\mathrm{ne}}$ and $s^* \in \mathrm{SOL}(G_{\mathrm{ds}}, U_{\mathrm{ds}})$. Moreover, $s(t) \in U_{\mathrm{ds}}$ for all $t \geq t_0$.

Proof: The proof is reported in Appendix I.

The above result concludes the convergence analysis. In fact, it shows that the physical system reaches an equilibrium, and such equilibrium is an NNE of the aggregative game solved by the proposed decision system, see Proposition 2. Thus, at the equilibrium, every DGU cannot obtain a decrement of its cost by unilaterally changing its state while satisfying the constraints.

Remark 6: Note that Proposition 2 and Theorem 1 show, respectively, that the state of the decision system (24d)–(24f) satisfies the coupling constraints in (9) at the steady state and the local constraints in (7) for all the time. Hence, the microgrid (4) in steady state satisfies both the local and coupling constraints in (7) and (9), while during transients they might be violated. However, we show in Section VI that when deviations occur, they remain within acceptable and safe ranges.

VI. SIMULATION

In this section, we test the proposed control framework in two different simulation scenarios. The first scenario consists of a four-DGU microgrid and is used to show the effectiveness and performance of the proposed scheme. The second scenario consists of a 16-DGU microgrid implemented by using the Simscape Electrical toolbox of MATLAB Simulink to model and simulate all the electrical and electronic components of a realistic microgrid. Therefore, this scenario aims at testing the scalability of the proposed framework in a large-scale and realistic microgrid.

A. Scenario 1: Four-DGU Microgrid

In this section, we consider a microgrid with $n = 4$ DGUs in a ring topology. Thus, $\mathcal{E}$ is composed of $m = 4$ transmission lines. The values of the parameters of each DGU and line are mainly taken from [12, Tables II and III]. Without loss

of generality, we set the reference values I^r, I_l^r, and u^r equal to $\mathbf{0}$, and $V^r = \text{col}(380.16, 381.21, 380.08, 380.13)$ [V] was randomly drawn within the interval $[380, 381.5]$. The minimum and maximum voltages for each DGU $i \in \mathcal{N}$ are set as $V_i^{\min} = 377$ [V] and $V_i^{\max} = 383$ [V], respectively, while for each transmission line $k \in \mathcal{E}$ we select $I_{l,k}^{\min} = -20$ [A] and $I_{l,k}^{\max} = 20$ [A]. The incidence matrix $B \in \mathbb{R}^{4\times 4}$ and Laplacian matrix $L_c \in \mathbb{R}^{4\times 4}$ are as follows:

$$B = \begin{bmatrix} 1 & 0 & 0 & 1 \\ -1 & 1 & 0 & 0 \\ 0 & -1 & 1 & 0 \\ 0 & 0 & -1 & -1 \end{bmatrix}$$

$$L_c = 200 \begin{bmatrix} 2 & -1 & 0 & -1 \\ -1 & 2 & -1 & 0 \\ 0 & -1 & 2 & -1 \\ -1 & 0 & -1 & 2 \end{bmatrix}.$$

Also, we select $\mathcal{E}_1 = \{1, 4\}$, $\mathcal{E}_2 = \{2\}$, $\mathcal{E}_3 = \{3\}$, and $\mathcal{E}_4 = \emptyset$. The values of the parameters of the objective function (12) of each DGU satisfy (18) and are reported in Table I. Furthermore, we set the parameters of the Cournot game as $p_r = 0.005$ [\$/(W · A)] and $\bar{p} = 2.5$ [\$/W], which satisfy Assumption 1. All the Lagrange multipliers' initial values are non-negative, and the maximum transmission line power loss is selected as $P_{\text{loss}}^{\max} = 35$ [W]. Moreover, we choose $\epsilon = 2$, $\varepsilon = 0.02$, and $\kappa = 0.1$. Then, (26) is satisfied for $c = 0.9$. Let the microgrid initial conditions be within the feasible set. Then, at $t = 5$ s, each current-type load $I_{L,i}$ and resistance-type load $Z_{L,i}$ are decreased by three units for all $i \in \mathcal{N}$. Note that the reduction of the impedance-type load implies that the load demand increases.

Remark 7: Theorem 2 ensures that the trajectory of (24) converges to (x^*, s^*). However, Theorem 2 does not guarantee any transient performance. Indeed, during transients, oscillations may arise. Then, to reduce such oscillations, we inject a dynamic damping term that is equal to zero at the steady state (see [14, eq. (8)]), thus not affecting the KKT conditions (19). Then, according to [14, eq. (8)], (24) can be modified as follows:

$$\boldsymbol{D}_x \dot{x} = Hx + Qu + \alpha_w Q(w - I) + d \tag{27a}$$
$$\boldsymbol{D}_w \dot{w} = I - w \tag{27b}$$
$$\varepsilon \dot{\eta} = -\eta - L_c \eta - L_c \nu + n\hat{I} \tag{27c}$$
$$\varepsilon \dot{\nu} = L_c \eta \tag{27d}$$
$$\kappa \dot{q} = \mathcal{T}_\Omega(q, -F_r(q, \eta) - \tilde{\boldsymbol{A}}^\top \boldsymbol{D}_r \lambda - \epsilon \Delta_q e_I) \tag{27e}$$
$$\kappa \dot{\lambda} = \mathcal{T}_{\mathbb{R}_+^{2m+2n+1}}\left(\lambda, \boldsymbol{D}_r\left(\boldsymbol{A}\hat{x} - b - \boldsymbol{L}_c \boldsymbol{D}_r \lambda - \boldsymbol{L}_c \theta\right)\right) \tag{27f}$$
$$\kappa \dot{\theta} = \boldsymbol{L}_c \boldsymbol{D}_r \lambda \tag{27g}$$

where $\alpha_w > 0$, $w \in \mathbb{R}^n$, and $\boldsymbol{D}_w \in \mathbb{R}^{n\times n}$ is a diagonal positive definite matrix. Note that the interconnection between (27a) and (27b) preserves the skew symmetry of the system, and the equilibrium is not affected. Moreover, the dynamics (27c)–(27g) are the same as (25), which implies that the convergence of the trajectory of (27) can be easily confirmed by using the following Lyapunov function[3]

$$S_e(x, s, w) = S(x, s) + \frac{\alpha_w}{2} \left\| w - w^* \right\|_{\boldsymbol{D}_w}^2. \tag{28}$$

In simulation, we select $\alpha_w = 0.8$ and $\boldsymbol{D}_w = 0.01\boldsymbol{I}$.

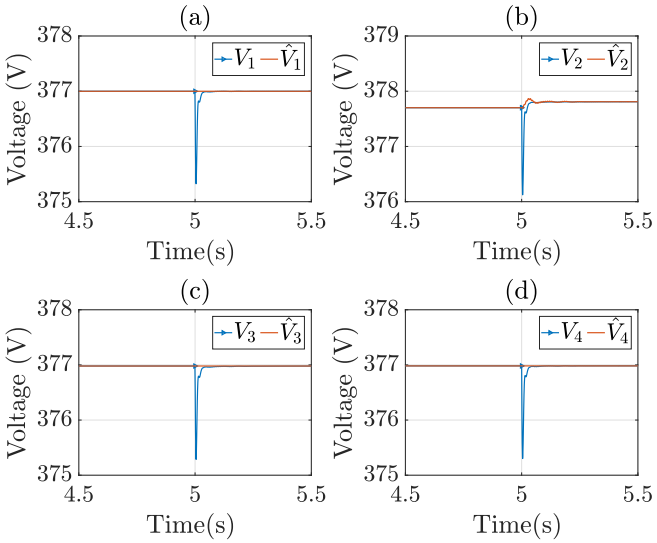

Fig. 3. (a)–(d) Comparison of the voltages $V_1, \ldots, V_4$ with the corresponding decision variables $\hat{V}_1, \ldots, \hat{V}_4$ generated by the decision system.

In Fig. 3, for each DGU $i \in \mathcal{N}$, we observe that when the load components $Z_{l,i}$ and $I_{L,i}$ have a step change, the voltage V_i remains stable and converges, after a short transient period, to the desired voltage value $\hat{V}_i$ generated by the decision system (27c). We also note that the voltage V_i of the DGU $i \in \mathcal{N}$ tracks very well the voltage reference $\hat{V}_i$ generated by the decision system, which evolves within the feasible interval $[377, 383]$ [V] for all the time. Moreover, we observe that when the microgrid voltages deviate from the corresponding references, they remain within acceptable and safe ranges. Specifically, they are within 5% of the nominal voltages $V_1^r, \ldots, V_4^r$, fulfilling, for instance, the standards for dc microgrids used as uninterruptible power supply systems for telecommunication applications [55].

In Fig. 4, for each DGU $i \in \mathcal{N}$, we observe that the current I_i has a similar transient as the voltage V_i, and then converges to the desired current value $\hat{I}_i$ generated by the decision system (27c).

Fig. 5 shows that the line current $I_{l,i}$ is stable and converges to the desired value $\hat{I}_{l,i}$ generated by the decision system (27c) for each DGU $i \in \mathcal{N}$, and remains within the feasible interval $[-20, 20]$ [A].

In Fig. 6, we show that the state of the decision system satisfies the local constraints in (8) all the time. In contrast, during transients, the state of the decision system might violate the coupling constraints in (9), as shown in Fig. 7(c) and (e). For the sake of completeness, in Fig. 7(b), (d), and (f),

[3]Note that the convergence analysis of the trajectory of (27) to a desired Nash equilibrium is similar to that in Section V-B. Also, the analysis of the damping dynamics (27b) is the same as in [14]. Since the main object of this article is to steer the considered dc microgrid to a desired Nash equilibrium, to prevent to divert the readers' attention from the main contribution of this article, then we prefer to not include the convergence analysis for (27).

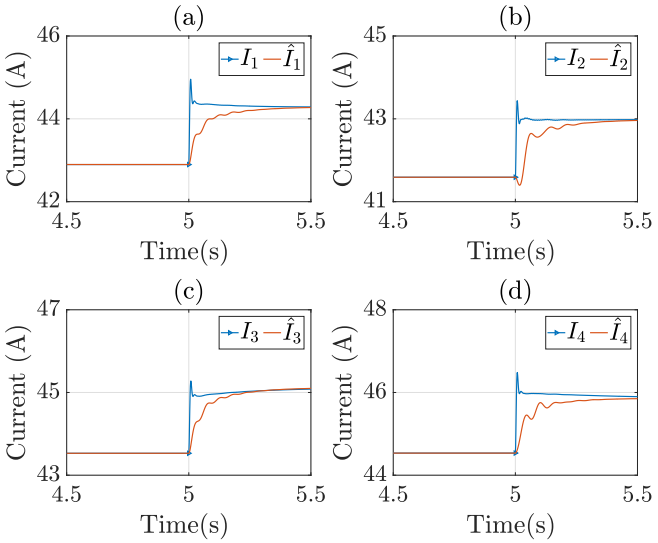

Fig. 4. (a)–(d) Comparison of the currents $I_1, \ldots, I_4$ with the corresponding decision variables $\hat{I}_1, \ldots, \hat{I}_4$ generated by the decision system.

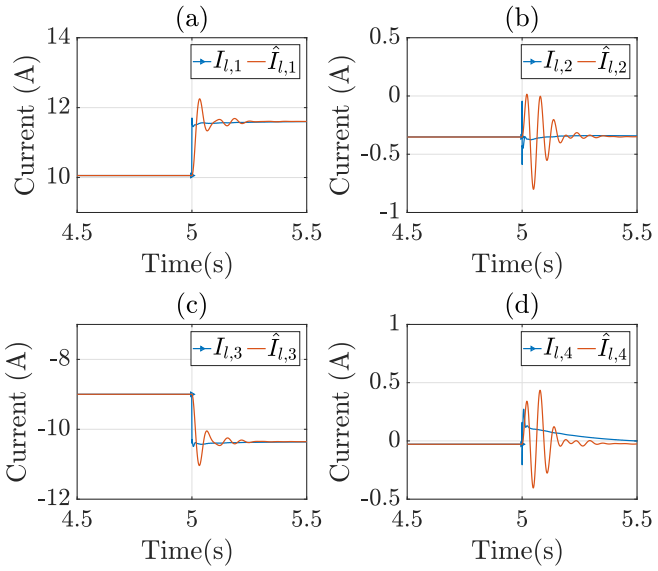

Fig. 5. (a)–(d) Comparison of the line currents $I_{l,1}, \ldots, I_{l,4}$ with the corresponding decision variables $\hat{I}_{l,1}, \ldots, \hat{I}_{l,4}$ generated by the decision system.

we show the time evolutions of the right-hand sides of (4), which express how much the microgrid state violates the constraints in (8) and (9). We can observe that the violation is very small and appears only during the transients to inevitably obey the physics dynamics in (4).

Moreover, in Fig. 7(a) we compare the estimation values $\eta_1, \ldots, \eta_4$ of the sum of the total generated current and its actual value σ_I, the effectiveness of the tracking depends on the choice of ε.

Fig. 8(a) shows the time evolution of the control inputs $u_1, \ldots, u_4$, while in Fig. 8(b) we observe that the injected damping $I - w$ converges to 0, as explained in Remark 7. The power loss in the transmission lines is within the predefined range, and its approximation $I_l^\top B^\top V^r$ well describes its actual value $I_l^\top B^\top V$ (see Fig. 9).

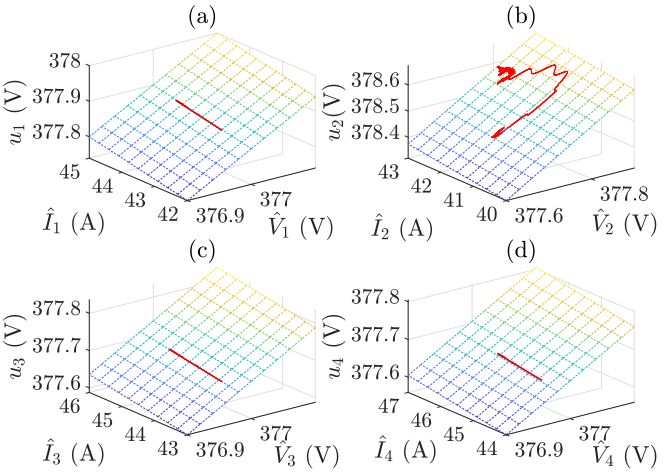

Fig. 6. (a)–(d) Trajectories of the decision system evolving on the local feasible set (8), i.e., $\hat{V} + R\hat{I} - u = \mathbf{0}$.

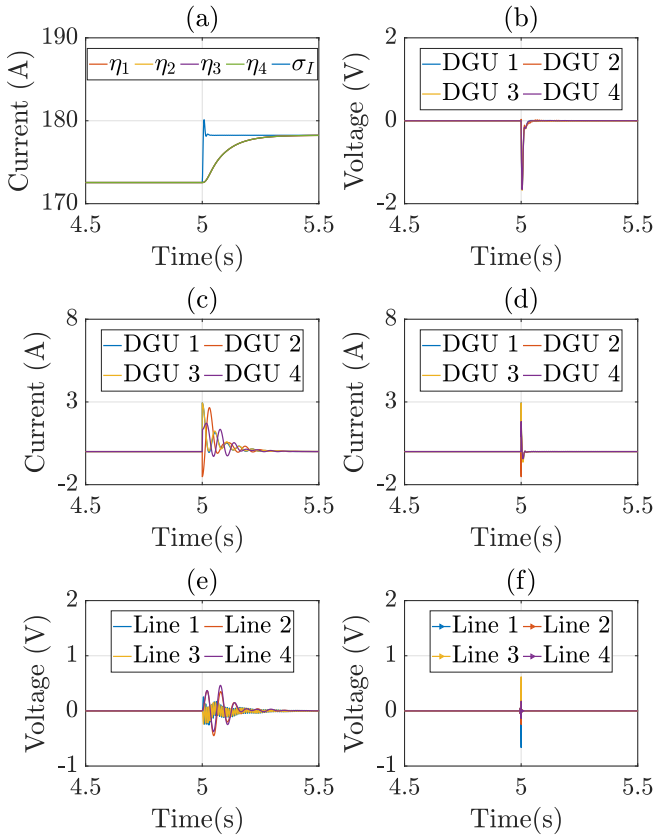

Fig. 7. (a) Comparison of the estimations of the total generated current $\eta_1, \ldots, \eta_4$ with its actual value σ_I. (b) Time evolution of the quantity $V + RI - u$. (c) Time evolution of the quantity $-\hat{I} - B\hat{I}_l + Z_L^{-1}\hat{V} + I_L$. (d) Time evolution of the quantity $-I - BI_l + Z_L^{-1}V + I_L$. (e) Time evolution of the quantity $R_l\hat{I}_l + B^\top\hat{V}$. (f) Time evolution of the quantity $R_l I_l + B^\top V$.

The simulation results in Figs. 3–9 confirm all the theoretical findings presented in Section V-B. Furthermore, the fast convergence of the closed-loop system trajectory indicates that the DGUs and decision system can reach a new NNE (e.g., associated with a load variation) within a relatively short time interval (in our case study less than 0.5 [s]).

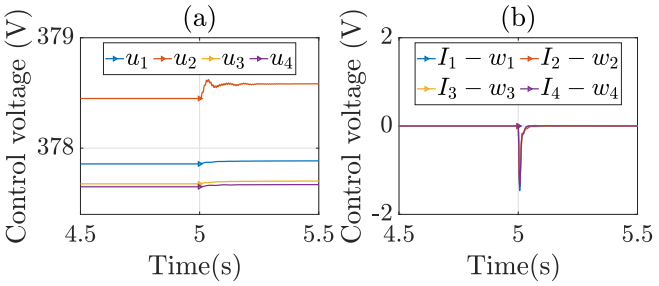

Fig. 8. (a) Control inputs $u_1, \ldots, u_4$. (b) Injected damping $I - w$ [see (27)].

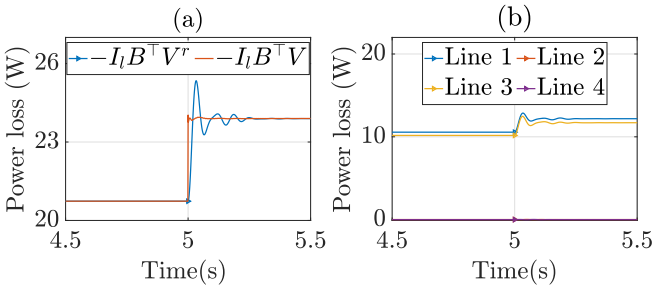

Fig. 9. (a) Comparison between the total approximated power loss and its actual value. (b) Approximated power loss in each line.

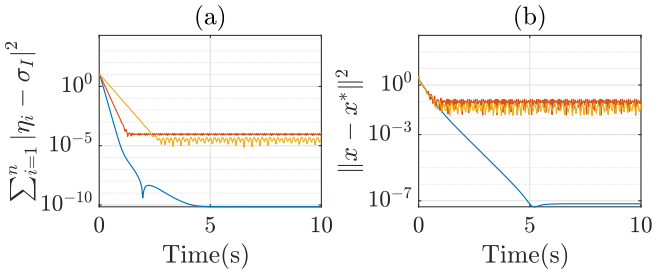

Fig. 10. (a) Estimation error. (b) Microgrid state error. Cases I, II, and III are in blue, red, and yellow, respectively.

In Fig. 10, we show the system evolution for different values of ε and κ, while keeping all the other parameters unchanged. Specifically, we consider the following three cases: 1) $\varepsilon = 0.05$ and $\kappa = 0.04$; 2) $\varepsilon = 0.10$ and $\kappa = 0.02$; and 3) $\varepsilon = 0.20$ and $\kappa = 0.01$. We observe that choosing a relatively small κ does not always lead to a faster convergence rate (see the paragraph below Theorem 1).

B. Scenario 2: 16-DGU Microgrid

In this section, we consider a dc microgrid containing 16 DGUs and 20 transmission lines. To simulate as much as possible a realistic microgrid, we have used the Simscape Electrical toolbox of MATLAB Simulink, and for the readers' convenience we have uploaded all the simulation files in [56]. Due to the page limit, we omit the details about the microgrid parameters and topology, which can be found in [56]. As in Scenario 1, we assume that each current-type load $I_{L,i}$ and resistance-type load $Z_{L,i}$ are increased by three units for all $i \in \mathcal{N}$ at $t = 5$ s.

Moreover, to show the effectiveness of the proposed control approach, we compare our results with those obtained by a modification of our controller, i.e., we replace the projection dynamics $\dot{q}$ (which is a component of $\dot{s}$) in the decision system (27e) by conventional primal–dual dynamics (see [57], [58]), i.e.,

$$\kappa \dot{q} = -F_r(q, \eta) - \tilde{\boldsymbol{A}}^\top \boldsymbol{D}_r \lambda - q_{\zeta,\mu} \tag{29a}$$
$$\kappa \dot{\zeta} = \hat{V} + R\hat{I} - u, \tag{29b}$$
$$\kappa \dot{\mu}_1 = \mathcal{T}_{\mathbb{R}^n_+}(\hat{V}, V^{\min} - \hat{V}) \tag{29c}$$
$$\kappa \dot{\mu}_2 = \mathcal{T}_{\mathbb{R}^n_+}(\hat{V}, \hat{V} - V^{\max}) \tag{29d}$$
$$\kappa \dot{\mu}_3 = \mathcal{T}_{\mathbb{R}^m_+}(\hat{I}, I_l^{\min} - \hat{I}_l) \tag{29e}$$
$$\kappa \dot{\mu}_4 = \mathcal{T}_{\mathbb{R}^m_+}(\hat{I}, \hat{I}_l - I_l^{\max}) \tag{29f}$$

where $\mu_1, \mu_2 \in \mathbb{R}^n$, $\mu_3, \mu_4 \in \mathbb{R}^m$, and $\zeta \in \mathbb{R}^n$ are the Lagrange multipliers of the local constraints in (7), and

$$q_{\zeta,\mu} \triangleq \operatorname{col}\left(\begin{bmatrix} -\zeta_i - \epsilon(I_i - \hat{I}_i) \\ R_i \zeta_i \\ \mu_{2,i} - \mu_{1,i} + \zeta_i \\ \mu_{4,i} - \mu_{3,i} \end{bmatrix}\right)_{i \in \mathcal{N}}.$$

For convenience and with a slight abuse of notation, the dynamics consisting of (27a)–(27d), (29), (27f), and (27g) will be denoted by (29) in the following.

Remark 8: Note that one can use the Lyapunov function

$$S_p(x, s, w, \zeta, \mu) = S_e(x, s, w) + \frac{1}{2}\|\zeta - \zeta^*\|^2 + \frac{1}{2}\|\mu - \mu^*\|^2$$

where $\mu \triangleq \operatorname{col}(\mu_1, \ldots, \mu_4)$, to analyze the trajectory convergence of (29).

Due to the page limit, we show only the trajectories of DGU 1 (the trajectories of the other DGUs are similar). Fig. 11(a) and (b) shows the control inputs generated by (27) and (29), respectively. By comparing Fig. 11(a) and (b), we can observe that (27) generates a much smoother control input than (29). Intuitively, such a result can be explained by the fact that the projection operator in the decision dynamics (27) constrains its trajectories to evolve within a manifold, thereby preserving the local constraints in (7). The same can be concluded from 11(c) and (d) for the microgrid voltages. Moreover, comparing Figs. 3 and 11(c), we observe that the scale of the microgrid does not significantly affect the convergence rate of the voltage trajectories, thus implying that our scheme has the potential to be used in large-scale microgrids.

Fig. 12 shows the deviation from the equilibrium of both the state of the microgrid and the state of the decision system, respectively, within the time interval [4.5, 5.5] s. We can observe that the trajectories obtained by implementing both (27) and (29) converge to the equilibrium after a short transient due to the loads step change. Comparing the blue trjactories with the red ones, we can conclude that the trajectories obtained by implementing (27) have a faster convergence rate than the ones obtained by implementing (29).

In conclusion, the simulation results in Figs. 11 and 12 show that employing in the decision system the projection dynamics instead of the primal–dual ones does not affect the convergence value but improves the transients in terms of faster convergence rate and less/smaller oscillations.

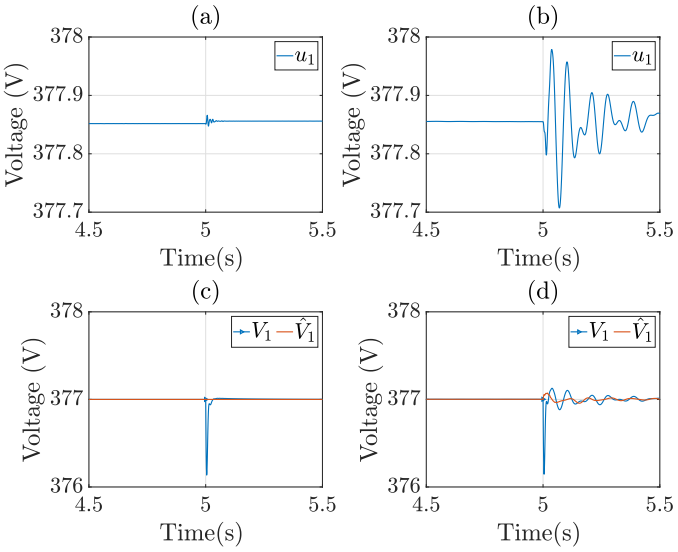

Fig. 11. (a) Control input generated by (27) based on projection dynamics. (b) Control input generated by (29) based on primal–dual dynamics. (c) Voltages of DGU 1 controlled by (27). (d) Voltages of DGU 1 controlled by (29).

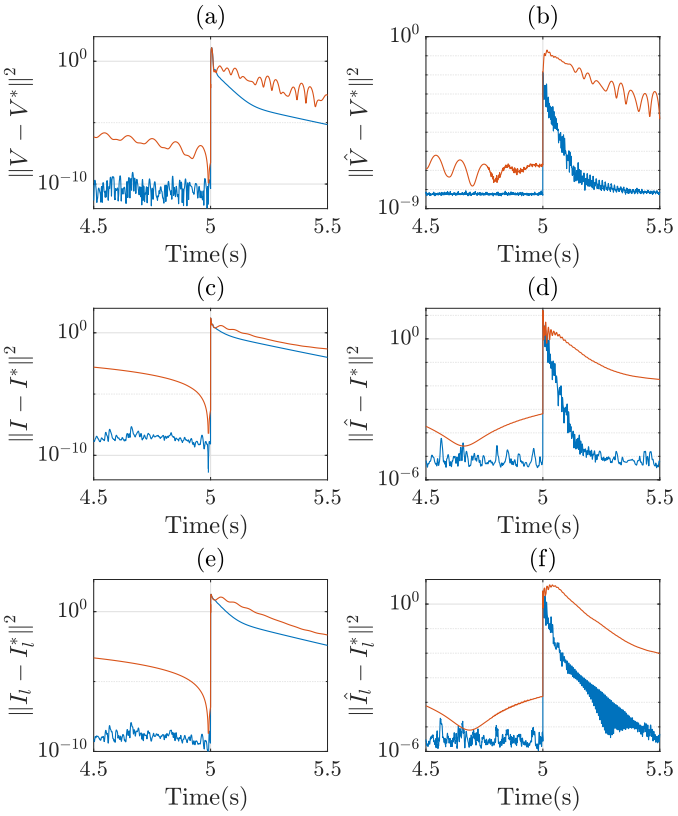

Fig. 12. (a), (c), and (e) Deviations of the microgrid states from the desired GNE (NNE). (b), (d), and (f) Deviations of the decision system states from the desired GNE (NNE). The blue trajectories are obtained by implementing (27), the red ones by implementing (29).

VII. Conclusion

We have formulated the electricity trading problem in dc microgrids as a Cournot GNE game subject to the microgrid dynamics. Then, employing concepts from projection dynamics and shifted passivity, we have developed a fully distributed continuous-time algorithm that solves the game and is able to drive the dc microgrid to an NNE satisfying predesigned objectives. Extensive and realistic numerical simulations show excellent performance of the designed control scheme.

From an energy management system viewpoint, the framework proposed in this article offers a solution to locally aggregate and consume the distributed generated energy. However, several avenues for future research remain unexplored. One potential direction for future work is to develop a discrete-time version of the proposed controller, e.g., building on the results in [59], to establish stronger robustness properties. Additionally, investigating the impact of distributed storage units on the energy trading could contribute to a more comprehensive understanding of the energy market dynamics. Finally, investigating a systematic procedure to select a suitable partition of the transmission lines could enhance the practical application of the proposed approach.

Appendix

A. Projection Operator

In this appendix, we introduce some properties of the projection operator. As in [51, eq. (2.13)], we denote the set of the inward normals at $x \in \Omega$ by

$$\mathcal{N}_\Omega^\star(x) = \{y \in -\mathcal{N}_\Omega(x) \mid \|y\| = 1\} \tag{30}$$

and $Y(x) = \arg\max_{y \in \mathcal{N}_\Omega^\star(x)} \{y^\top F(x)\}$. Thus, (2) satisfies

$$\mathcal{T}_\Omega(x, -F(x)) = -F(x) + Q(x)\, Y(x) \tag{31}$$

where $Q(x) = \max\{0, (Y(x))^\top F(x)\}$. From (2), the following equality holds for the projection on the tangent cone:

$$\mathcal{T}_\Omega(x, -F(x)) = \mathcal{P}_{T_\Omega(x)}(-F(x)) \tag{32}$$

where $T_\Omega(x)$ represents the tangent cone of Ω at $x \in \Omega$. If $\mathcal{T}_\Omega(x, -F(x)) = 0$ for $x \in \Omega$, then it follows that

$$\begin{cases} F(x) = 0, & \text{if } x \in \operatorname{int}(\Omega) \\ F(x) = Q(x)\, Y(x), & \text{if } F(x) \in -\mathcal{N}_\Omega(x). \end{cases} \tag{33}$$

Hence, if Ω is a convex polyhedron, the solution x solving $\mathcal{T}_\Omega(x, -F(x)) = 0$ coincides with the solution of the VI(F, Ω) [51, Th. 2.4].

B. Proof of Lemma 1

By taking the time derivative of (6) along the trajectory of (5), it follows

$$\begin{aligned} \dot{E}(x) &= \left(x - x^*\right)^\top \left(Hx + Hu - Hx^* + Hu^*\right) \\ &\le \left(u - u^*\right)^\top \left(I - I^*\right) \end{aligned} \tag{34}$$

where the last inequality uses the fact that H is the difference between an antisymmetric matrix and a diagonal positive definite matrix. ■

C. Proof of Lemma 2

According to [38, Proposition 2.3.2.c], F_r is strongly monotone if and only if its Jacobian $J_{F_r}(u, x, \sigma_I \mathbf{1}) \succ 0$. For each DGU $i \in \mathcal{N}$, f_i in (12) is linear-quadratic [see (12b)], and thus strongly convex with respect to all arguments (x_i, u_i) except for I_i, due to (12c). From this and the given particular form of (12), proving that F_r is strongly monotone reduces to show that

$$y_I^\top \frac{\partial F_r(u, x, \sigma_I \mathbf{1})}{\partial I} y_I = y_I^\top S y_I > 0 \tag{35}$$

holds for all $y_I \in \mathbb{R}^n$, where S represents the symmetric part of $\partial F_r(u, x, \sigma_I \mathbf{1})/\partial I$, which reads as

$$S \triangleq \begin{bmatrix} r_1 \alpha_{I_1} + 2 r_1 p_r V_1^r & \cdots & \frac{1}{2}\left(r_1 p_r V_1^r + r_n p_r V_n^r\right) \\ \vdots & \ddots & \vdots \\ \frac{1}{2}\left(r_n p_r V_n^r + r_1 p_r V_1^r\right) & \cdots & r_n \alpha_{I_n} + 2 r_n p_r V_n^r \end{bmatrix}.$$

The inequality (18) implies that the following inequality

$$r_i \alpha_{I_i} + 2 r_i p_r V_i^r - \frac{n-1}{2} r_i p_r V_i^r - \frac{1}{2} \sum_{j \neq i} r_j p_r V_j^r > 0$$

holds for all $i \in \mathcal{N}$, which implies that S is a symmetric diagonally dominant matrix with positive entries. Hence, $S \succ 0$, which concludes the proof. ∎

D. Proof of Proposition 1

From the definition in (19), we can rewrite G_r as the sum of two operators

$$\mathfrak{A} : z \mapsto \begin{bmatrix} F_r(q, \sigma_I \mathbf{1}) \\ \boldsymbol{D}_r \boldsymbol{L}_c \boldsymbol{D}_r \lambda - \boldsymbol{b} \\ \mathbf{0} \end{bmatrix}$$

$$\mathfrak{B} : z \mapsto \begin{bmatrix} \mathbb{0} & \tilde{\boldsymbol{A}}^\top \boldsymbol{D}_r & \mathbb{0} \\ -\boldsymbol{D}_r \boldsymbol{A} & \mathbb{0} & \boldsymbol{D}_r \boldsymbol{L}_c \\ \mathbb{0} & -\boldsymbol{L}_c \boldsymbol{D}_r & \mathbb{0} \end{bmatrix} z.$$

Since $\boldsymbol{D}_r$ is positive definite, we can follow the same steps as in [29, Lemma 1] to prove that $\mathfrak{B}$ is maximally monotone and $\mathfrak{A}$ is cocoercive and thus maximally monotone [60, Example 20.31]. Since the sum of two maximally monotone operators is maximally monotone, this concludes the proof. ∎

E. Proof of Proposition 2

The proof of each statement of Proposition 2 is reported in the following.

1) Note that $(u^*, \hat{x}^*) \in K_\Omega$ implies that $H\hat{x}^* + Qu^* + d = \mathbf{0}$. Then, since H in (5) is full rank, we can deduce that

$$Hx^* + Qu^* + d = H\hat{x}^* + Qu^* + d = \mathbf{0} \tag{36}$$

which implies that $x^* = \hat{x}^*$ and thus $I^* = \hat{I}^*$. According to (23), it follows that $\eta_i^* = \sum_{i=1}^n \hat{I}_i^* \triangleq \sigma_I^*$ holds for all $i \in \mathcal{N}$. By substituting these equalities in (24d), we can deduce that

$$F_r(q^*, \eta^*) = F_r(q^*, \sigma_I^* \mathbf{1}), \quad \mathcal{T}_U(\hat{z}^*, -G_r(\hat{z}^*)) = \mathbf{0}. \tag{37}$$

By combining Lemma 3 with the analysis in [51, Th. 2.4], it follows that $\hat{z}^*$ solves the VI(G_r, U), and $x^* = \hat{x}^* = x^{\text{ne}}$, $u^* = u^{\text{ne}}$, and $\lambda^* = \lambda^{\text{ne}}$. Using the assumption that $V^r \notin \text{span}\{\mathbf{1}\}$ and following a reasoning akin to that in Remark 2, we confirm that (u^*, x^*, λ^*) is unique.

2) Based on the above equalities, we can deduce that

$$\mathcal{T}_{U_{\text{ds}}}\left(s^*, -G_{\text{ds}}(s^*) - \epsilon \Delta_{s^*} e_I^*\right) = \mathcal{T}_{U_{\text{ds}}}\left(s^*, -G_{\text{ds}}(s^*)\right) = \mathbf{0} \tag{38}$$

where $e_I^* = I^* - \hat{I}^*$. The above equality (38) confirms that $s^* \in \text{SOL}(G_{\text{ds}}, U_{\text{ds}})$. ∎

F. Proof of Corollary 1

Multiplying both sides of (24f) by $\mathbf{1}^\top \otimes \boldsymbol{I}$, it follows that the following equalities

$$(\mathbf{1}^\top \otimes \boldsymbol{I})\dot{\theta} = \mathbf{0}, \quad (\mathbf{1}^\top \otimes \boldsymbol{I})\theta^* = (\mathbf{1}^\top \otimes \boldsymbol{I})\theta(t_0) \tag{39}$$

hold if the trajectory of (24) converges to $s^* \in \text{SOL}(G_{\text{ds}}, U_{\text{ds}})$. Recall that $s^* \in \text{SOL}(G_{\text{ds}}, U_{\text{ds}})$ implies that s^* is the solution of the KKT condition (19). Based on the Lagrange dual theory [48, Sec. 5], s^* is the solution of the following augmented dual problem:

$$\max_{\theta} \min_{\lambda \in \mathbb{R}_+^{2m+2n+1}} \sum_{i=1}^n r_i \left(-f_i^*(A_i^\top \lambda_i) + \lambda_i^\top b_i\right) + \theta^\top \boldsymbol{L}_c \boldsymbol{D}_r \lambda + \tfrac{1}{2}\|\boldsymbol{D}_r \lambda\|_{\boldsymbol{L}_c}^2 \tag{40}$$

where for all $i \in \mathcal{N}$

$$f_i^*(-A_i^\top \lambda_i) = \max_{(u_i, x_i) \in \Omega_i} -f_i(u_i, x_i, \bar{\sigma}_i) - \lambda_i^\top A_i x_i$$

denotes the conjugate of f_i (see [61, Sec. A]), and $\bar{\sigma}_i$ is defined below (14). Employing [61, Proposition 12.60], it follows that the objective function of (40) is strongly convex with respect to $\boldsymbol{D}_r \boldsymbol{L}_c \theta$. Hence, $\boldsymbol{D}_r \boldsymbol{L}_c \theta^*$ has a unique value. Since $\boldsymbol{D}_r \boldsymbol{L}_c + \mathbf{1}^\top \otimes \boldsymbol{I}$ is full rank, θ^* satisfying (39) is unique. ∎

G. Proof of Proposition 3

Let $\hat{s} \triangleq \text{col}(\eta, \nu, u, \hat{x}, \lambda, \theta)$. Compared with s, $\hat{s}$ simply rearranges the components of s. Following the proof in Lemma 2, $\boldsymbol{D}_s^{-1}(G_{\text{ds}}(s) + \epsilon \Delta_s e_I)$ is monotone with respect to s if and only if the following condition

$$y_{\hat{s}}^\top A_{\hat{s}} y_{\hat{s}} \geq 0, \quad A_{\hat{s}} \triangleq \boldsymbol{D}_s^{-1} \frac{\partial\left(G_{\text{ds}}(s) + \epsilon \Delta_s e_I\right)}{\partial \hat{s}} \tag{41}$$

holds for all $y_{\hat{s}} \in \mathbb{R}^{|\hat{s}|}$. Since we have

$$\frac{1}{2}(A_{\hat{s}} + A_{\hat{s}}^\top) = \begin{bmatrix} A_o & \mathbb{0} & \mathbb{0} \\ \mathbb{0} & \frac{1}{\kappa} \boldsymbol{D}_r \boldsymbol{L}_c \boldsymbol{D}_r & \mathbb{0} \\ \mathbb{0} & \mathbb{0} & \mathbb{0} \end{bmatrix}$$

then we can deduce that the symmetric part of $A_{\hat{s}}$ is positive semidefinite if the following matrix

$$A_o \triangleq \begin{bmatrix} \frac{1}{\varepsilon}(\boldsymbol{I}+L_c) & \mathbb{0} & -\frac{n}{\varepsilon}\frac{\partial \hat{I}}{\partial \hat{x}} \\ \mathbb{0} & \frac{1}{\kappa}\frac{\partial F_r(q,\eta)}{\partial u} & -\frac{\epsilon}{\kappa}\frac{\partial \hat{I}}{\partial \hat{x}} \\ \frac{1}{\kappa}\frac{\partial F_r(q,\eta)}{\partial \eta} & \mathbb{0} & \frac{1}{\kappa}\frac{\partial F_r(q,\eta)}{\partial \hat{x}} \end{bmatrix}$$

is positive semidefinite. Involving the fact that L_c is positive semidefinite, it follows that the symmetric part of A_o is positive semidefinite if

$$\sum_{i=1}^{n}\left\{\frac{1}{\varepsilon}y_{\eta_i}^2-\left(\frac{n}{\varepsilon}-\frac{1}{\kappa}r_i p_r V_i^r\right)y_{\eta_i}y_{\hat{I}_i}+\frac{c}{\kappa}\left(r_i\alpha_{I_i}+r_i p_r V_i^r\right)y_{\hat{I}_i}^2\right\}$$

$$+\sum_{i=1}^{n}\left\{\frac{1}{\kappa}r_i\alpha_{u_i}y_{u_i}^2-\frac{\epsilon}{\kappa}y_{u_i}y_{\hat{I}_i}+\frac{1-c}{\kappa}\left(r_i\alpha_{I_i}+r_i p_r V_i^r\right)y_{\hat{I}_i}^2\right\}\geq 0$$

holds for all $y_{\eta_i}, y_{u_i}, y_{\hat{I}_i}\in\mathbb{R}$. Completing the square, we can deduce that the symmetric part of A_o is positive semidefinite if the condition (26) holds. ∎

H. Proof of Theorem 1

The proof of each statement of Theorem 1 is reported in the following.

1) The result follows from the definition and properties of the tangent cone operator [51, eq. (2.14)].
2) For convenience, we rewrite the systems (24b) and (24c) and (24d)–(24f) in the following compact form:

$$\varepsilon\dot{\gamma}=A_e\gamma+B_e\hat{I},\quad \kappa\dot{\hat{z}}=\mathcal{T}_U\left(\hat{z},-G_e\left(\hat{z},\eta\right)-\epsilon\Delta_{\hat{z}}e_I\right)$$

where $\gamma\triangleq\mathrm{col}(\eta,\nu)$, A_e and B_e are constant matrices, and G_e can be easily attained by inspection of (24d)–(24f). Following the definitions in (30) and (31), and using the same notation for the operators, we define

$$Y_U(\hat{z})=\underset{y\in\mathcal{N}_U^{\star}(\hat{z})}{\arg\max}\left\{y^{\top}\left(G_e\left(\hat{z},\eta\right)+\epsilon\Delta_{\hat{z}}e_I\right)\right\}$$

$$Q_U(\hat{z})=\max\left\{0,\left(Y_U\left(\hat{z}\right)\right)^{\top}\left(G_e\left(\hat{z},\eta\right)+\epsilon\Delta_{\hat{z}}e_I\right)\right\}.$$

Exploiting the geometric properties of the normal cone, discussed in Section I-D2, it follows that for all $\hat{z},\hat{z}^*\in U$ it holds that

$$\left(\hat{z}-\hat{z}^*\right)^{\top}Q_U\left(\hat{z}\right)Y_U\left(\hat{z}\right)\leq 0. \tag{42}$$

Taking the time derivative of $W(s)$, we have

$$\begin{aligned}\dot{W}(s)=&-\frac{1}{\kappa}\left(\hat{z}-\hat{z}^*\right)^{\top}\left(G_e\left(\hat{z},\eta\right)-Q_U\left(\hat{z}\right)Y_U\left(\hat{z}\right)\right)\\&+\frac{1}{\varepsilon}\left(\gamma-\gamma^*\right)^{\top}\left(A_e\gamma+B_e\hat{I}\right)\\&+\frac{\epsilon}{\kappa}\left(u-u^*\right)^{\top}\left(\left(\hat{I}-\hat{I}^*\right)-\left(I-I^*\right)\right).\end{aligned} \tag{43}$$

By involving the first equality in (37), we can deduce that $G_e(\hat{z}^*,\eta^*)=G_r(\hat{z}^*)$. Hence, it follows that

$$\left(\hat{z}-\hat{z}^*\right)^{\top}G_e\left(\hat{z}^*,\eta^*\right)=\left(\hat{z}-\hat{z}^*\right)^{\top}G_r\left(\hat{z}^*\right)\geq 0. \tag{44}$$

By combining (42)–(44) with the equality $A_e\gamma^*+B_e\hat{I}^*=\mathbf{0}$, we conclude that

$$\begin{aligned}\dot{W}(s)\leq&-\left(s-s^*\right)^{\top}\boldsymbol{D}_s^{-1}\left(G_{\mathrm{ds}}(s)-G_{\mathrm{ds}}\left(s^*\right)\right)\\&+\left(s-s^*\right)^{\top}\boldsymbol{D}_s^{-1}(\epsilon\Delta_s\hat{I}-\epsilon\Delta_{s^*}\hat{I}^*)\\&-\left(s-s^*\right)^{\top}\boldsymbol{D}_s^{-1}\left(\epsilon\Delta_s I-\epsilon\Delta_{s^*}I^*\right)\\\leq&-\frac{\epsilon}{\kappa}\left(u-u^*\right)^{\top}\left(I-I^*\right)\end{aligned} \tag{45}$$

where the last inequality follows by noting that $\Delta_s=\Delta_{s^*}$ and exploiting the monotonicity of $\boldsymbol{D}_s^{-1}(G_{\mathrm{ds}}(s)+\epsilon\Delta_s e_I)$ with respect to s (see Proposition 3), which implies the monotonicity of $\boldsymbol{D}_s^{-1}(G_{\mathrm{ds}}(s)-\epsilon\Delta_s\hat{I})$ with respect to s. ∎

I. Proof of Theorem 2

Construct the following Lyapunov function

$$S(x,s)=\frac{\epsilon}{\kappa}E(x)+W(s). \tag{46}$$

Taking the time derivative of $S(x,s)$ and combining Lemma 1 and Theorem 1, it follows that

$$\begin{aligned}\dot{S}(x,s)\leq&\frac{\epsilon}{\kappa}\left(u-u^*\right)^{\top}\left(I-I^*\right)\\&-\frac{\epsilon}{\kappa}\left(u-u^*\right)^{\top}\left(I-I^*\right)=0\end{aligned} \tag{47}$$

where the first inequality invokes (34) and (45). Construct the following level set

$$\Omega_c\triangleq\left\{(x,s)\in\mathbb{R}^{2n+m}\times U_{\mathrm{ds}}\mid S(x,s)\leq S(x_0,s_0)\right\}.$$

Note that x^* and s^* are bounded, S is continuous, and the inequality in (47) proves that $\dot{S}(x,s)$ is nonincreasing for all $t\geq t_0$. Hence, we deduce that Ω_c is a compact set that is positively invariant with respect to (24). Exploiting the first equality of (34) and the first inequality of (45), it follows that

$$\begin{aligned}\dot{S}(x,s)\leq&-\frac{1}{\varepsilon}\left\|\eta-\eta^*\right\|^2+\frac{n}{\varepsilon}\left(\eta-\eta^*\right)^{\top}\left(\hat{I}-\hat{I}^*\right)\\&-\frac{1}{\kappa}\left(q-q^*\right)^{\top}\left(F_r(q,\eta)-F_r\left(q^*,\eta^*\right)\right)\\&+\frac{\epsilon}{\kappa}\left(u-u^*\right)^{\top}\left(\hat{I}-\hat{I}^*\right)-\frac{1}{\varepsilon}\left\|\eta-\eta^*\right\|_{L_c}^2\\&-\frac{1}{\kappa}\left(\lambda-\lambda^*\right)^{\top}\boldsymbol{D}_r\boldsymbol{L}_c\boldsymbol{D}_r\left(\lambda-\lambda^*\right)\\&+\frac{\epsilon}{\kappa}\left(x-x^*\right)^{\top}H\left(x-x^*\right).\end{aligned} \tag{48}$$

Since the symmetric part of A_o is positive semidefinite [under condition (26)] and leveraging [38, Proposition 2.3.2.c], we conclude that the sum of the first four items of the right-hand side of (48) is negative semidefinite. Based on such a fact, (48) becomes

$$\begin{aligned}\dot{S}(x,s)\leq&-\frac{1}{\kappa}\left(\lambda-\lambda^*\right)^{\top}\boldsymbol{D}_r\boldsymbol{L}_c\boldsymbol{D}_r\left(\lambda-\lambda^*\right)\\&-\frac{1}{\varepsilon}\left\|\eta-\eta^*\right\|_{L_c}^2+\frac{\epsilon}{\kappa}\left(x-x^*\right)^{\top}H\left(x-x^*\right).\end{aligned} \tag{49}$$

Note that $\boldsymbol{D}_r \boldsymbol{L}_c \boldsymbol{D}_r \succeq 0$, $L_c \succeq 0$, 0 and $\mathbf{1}$ are the eigenpair of L_c, and H is negative definite. Hence, combining these facts, Proposition 2(1), and (49), we conclude that $\dot{S}(x,s) = 0$ if and only if $x = x^*$, $\hat{x} = \hat{x}^*$, $\eta \in \operatorname{span}(\mathbf{1}_n)$, and $r_1\lambda_1 = \cdots = r_n\lambda_n$. These conditions imply that $\dot{S}(x,s) = 0$ if and only if $\dot{x} = \mathbf{0}$ and $\dot{s} = \mathbf{0}$, and thus confirms that the following set

$$\Omega_m \triangleq \left\{(x,s) \in \mathbb{R}^{2n+m} \times U_{\mathrm{ds}} \mid \dot{x} = \mathbf{0}, \dot{s} = \mathbf{0}\right\}$$

is the largest invariant set within

$$\Omega_e \triangleq \left\{(x,s) \in \mathbb{R}^{2n+m} \times U_{\mathrm{ds}} \mid \dot{S}(x,s) = 0\right\}.$$

We conclude the proof by invoking Proposition 2 and LaSalle's invariance principle [54, Th. 4.4] which imply that the trajectory of (24) converges to the Ω_m, $x^* = \hat{x}^* = \hat{x}^{\mathrm{ne}}$, and $s^* \in \mathrm{SOL}(G_{\mathrm{ds}}, U_{\mathrm{ds}})$. ∎

REFERENCES

[1] Z. Fu, M. Cucuzzella, C. Cenedese, W. Yu, and J. M. Scherpen, "A distributed control framework for the optimal operation of DC microgrids," in *Proc. IEEE 61st Conf. Decis. Control (CDC)*, Dec. 2022, pp. 4585–4590.

[2] X. He, J. Yu, T. Huang, and C. Li, "Distributed power management for dynamic economic dispatch in the multimicrogrids environment," *IEEE Trans. Control Syst. Technol.*, vol. 27, no. 4, pp. 1651–1658, Jul. 2019.

[3] C. Li, X. Yu, T. Huang, and X. He, "Distributed optimal consensus over resource allocation network and its application to dynamical economic dispatch," *IEEE Trans. Neural Netw. Learn. Syst.*, vol. 29, no. 6, pp. 2407–2418, Jun. 2018.

[4] W. Yu, C. Li, X. Yu, G. Wen, and J. Lü, "Economic power dispatch in smart grids: A framework for distributed optimization and consensus dynamics," *Sci. China Inf. Sci.*, vol. 61, no. 1, pp. 1–16, Jan. 2018.

[5] L. Meng et al., "Review on control of DC microgrids and multiple microgrid clusters," *IEEE J. Emerg. Sel. Topics Power Electron.*, vol. 5, no. 3, pp. 928–948, Sep. 2017.

[6] F. Dörfler, S. Bolognani, J. W. Simpson-Porco, and S. Grammatico, "Distributed control and optimization for autonomous power grids," in *Proc. 18th Eur. Control Conf. (ECC)*, 2019, pp. 2436–2453.

[7] P. Monshizadeh, J. E. Machado, R. Ortega, and A. van der Schaft, "Power-controlled Hamiltonian systems: Application to electrical systems with constant power loads," *Automatica*, vol. 109, Nov. 2019, Art. no. 108527.

[8] P. Nahata, R. Soloperto, M. Tucci, A. Martinelli, and G. Ferrari-Trecate, "A passivity-based approach to voltage stabilization in DC microgrids with ZIP loads," *Automatica*, vol. 113, Mar. 2020, Art. no. 108770.

[9] K. C. Kosaraju, M. Cucuzzella, J. M. A. Scherpen, and R. Pasumarthy, "Differentiation and passivity for control of Brayton–Moser systems," *IEEE Trans. Autom. Control*, vol. 66, no. 3, pp. 1087–1101, Mar. 2021.

[10] J. Ferguson, M. Cucuzzella, and J. M. A. Scherpen, "Exponential stability and local ISS for DC networks," *IEEE Control Syst. Lett.*, vol. 5, no. 3, pp. 893–898, Jul. 2021.

[11] M. Cucuzzella, K. C. Kosaraju, and J. M. A. Scherpen, "Voltage control of DC microgrids: Robustness for unknown ZIP-loads," *IEEE Control Syst. Lett.*, vol. 7, pp. 139–144, 2023.

[12] M. Cucuzzella, S. Trip, C. De Persis, X. Cheng, A. Ferrara, and A. van der Schaft, "A robust consensus algorithm for current sharing and voltage regulation in DC microgrids," *IEEE Trans. Control Syst. Technol.*, vol. 27, no. 4, pp. 1583–1595, Jul. 2019.

[13] M. Tucci, L. Meng, J. M. Guerrero, and G. Ferrari-Trecate, "Stable current sharing and voltage balancing in DC microgrids: A consensus-based secondary control layer," *Automatica*, vol. 95, pp. 1–13, Sep. 2018.

[14] S. Trip, M. Cucuzzella, X. Cheng, and J. Scherpen, "Distributed averaging control for voltage regulation and current sharing in DC microgrids," *IEEE Control Syst. Lett.*, vol. 3, no. 1, pp. 174–179, Jan. 2019.

[15] J. Ferguson, M. Cucuzzella, and J. M. A. Scherpen, "Increasing the region of attraction in DC microgrids," *Automatica*, vol. 151, May 2023, Art. no. 110883.

[16] Y. Kawano, M. Cucuzzella, S. Feng, and J. M. A. Scherpen, "Krasovskii and shifted passivity based output consensus," *Automatica*, vol. 155, Sep. 2023, Art. no. 111167.

[17] M. B. Shadmand and R. S. Balog, "Multi-objective optimization and design of photovoltaic-wind hybrid system for community smart DC microgrid," *IEEE Trans. Smart Grid*, vol. 5, no. 5, pp. 2635–2643, Sep. 2014.

[18] S. Moayedi and A. Davoudi, "Unifying distributed dynamic optimization and control of islanded DC microgrids," *IEEE Trans. Power Electron.*, vol. 32, no. 3, pp. 2329–2346, Mar. 2017.

[19] W. Su, S. S. Yu, H. Li, H. H. Iu, and T. Fernando, "An MPC-based dual-solver optimization method for DC microgrids with simultaneous consideration of operation cost and power loss," *IEEE Trans. Power Syst.*, vol. 36, no. 2, pp. 936–947, Mar. 2021.

[20] M. Cucuzzella et al., "Distributed control of DC grids: Integrating prosumers' motives," *IEEE Trans. Power Syst.*, vol. 37, no. 4, pp. 3299–3310, Jul. 2022.

[21] Y. Dou, M. Chi, Z.-W. Liu, G. Wen, and Q. Sun, "Distributed secondary control for voltage regulation and optimal power sharing in DC microgrids," *IEEE Trans. Control Syst. Technol.*, vol. 30, no. 6, pp. 2561–2572, Nov. 2022.

[22] T. Yang et al., "A survey of distributed optimization," *Annu. Rev. Control*, vol. 47, pp. 278–305, Jan. 2019.

[23] A. Nedic, A. Olshevsky, and W. Shi, "Achieving geometric convergence for distributed optimization over time-varying graphs," *SIAM J. Optim.*, vol. 27, no. 4, pp. 2597–2633, Jan. 2017.

[24] H. Liu, W. Yu, and G. Chen, "Discrete-time algorithms for distributed constrained convex optimization with linear convergence rates," *IEEE Trans. Cybern.*, vol. 52, no. 6, pp. 4874–4885, Jun. 2022.

[25] Y. Zhu, W. Yu, G. Wen, G. Chen, and W. Ren, "Continuous-time distributed subgradient algorithm for convex optimization with general constraints," *IEEE Trans. Autom. Control*, vol. 64, no. 4, pp. 1694–1701, Apr. 2019.

[26] Y. Zhu, W. Ren, W. Yu, and G. Wen, "Distributed resource allocation over directed graphs via continuous-time algorithms," *IEEE Trans. Syst., Man, Cybern., Syst.*, vol. 51, no. 2, pp. 1097–1106, Feb. 2021.

[27] G. Belgioioso and S. Grammatico, "Semi-decentralized Nash equilibrium seeking in aggregative games with separable coupling constraints and non-differentiable cost functions," *IEEE Control Syst. Lett.*, vol. 1, no. 2, pp. 400–405, Oct. 2017.

[28] C. Cenedese, G. Belgioioso, S. Grammatico, and M. Cao, "Time-varying constrained proximal type dynamics in multi-agent network games," in *Proc. Eur. Control Conf. (ECC)*, May 2020, pp. 148–153.

[29] C. Cenedese, G. Belgioioso, S. Grammatico, and M. Cao, "An asynchronous distributed and scalable generalized Nash equilibrium seeking algorithm for strongly monotone games," *Eur. J. Control*, vol. 58, pp. 143–151, Mar. 2021.

[30] C. De Persis and S. Grammatico, "Continuous-time integral dynamics for a class of aggregative games with coupling constraints," *IEEE Trans. Autom. Control*, vol. 65, no. 5, pp. 2171–2176, May 2020.

[31] C. De Persis and S. Grammatico, "Distributed averaging integral Nash equilibrium seeking on networks," *Automatica*, vol. 110, Dec. 2019, Art. no. 108548.

[32] M. Ye and G. Hu, "Distributed Nash equilibrium seeking by a consensus based approach," *IEEE Trans. Autom. Control*, vol. 62, no. 9, pp. 4811–4818, Sep. 2017.

[33] J. Koshal, A. Nedic, and U. V. Shanbhag, "Distributed algorithms for aggregative games on graphs," *Oper. Res.*, vol. 64, no. 3, pp. 680–704, Jun. 2016.

[34] A. R. Romano and L. Pavel, "Dynamic NE seeking for multi-integrator networked agents with disturbance rejection," *IEEE Trans. Control Netw. Syst.*, vol. 7, no. 1, pp. 129–139, Mar. 2020.

[35] M. Bianchi and S. Grammatico, "Continuous-time fully distributed generalized Nash equilibrium seeking for multi-integrator agents," *Automatica*, vol. 129, Jul. 2021, Art. no. 109660.

[36] F. Parise, M. Colombino, S. Grammatico, and J. Lygeros, "Mean field constrained charging policy for large populations of plug-in electric vehicles," in *Proc. 53rd IEEE Conf. Decis. Control*, Dec. 2014, pp. 5101–5106.

[37] C. Cenedese, F. Fabiani, M. Cucuzzella, J. M. A. Scherpen, M. Cao, and S. Grammatico, "Charging plug-in electric vehicles as a mixed-integer aggregative game," in *Proc. IEEE 58th Conf. Decis. Control (CDC)*, Dec. 2019, pp. 4904–4909.

[38] F. Facchinei and J.-S. Pang, *Finite-Dimensional Variational Inequalities and Complementarity Problems*. Berlin, Germany: Springer, 2003.

[39] A. Caramizaru and A. Uihlein, "Energy communities: An overview of energy and social innovation," Sci. Anal. Rev., Publications Office Eur. Union, Luxembourg, Tech. Rep., Policy Assessment KJ-NA-30083-EN-N, 2020.

[40] R. Trevisan, E. Ghiani, and F. Pilo, "Renewable energy communities in positive energy districts: A governance and realisation framework in compliance with the Italian regulation," *Smart Cities*, vol. 6, no. 1, pp. 563–585, Feb. 2023.

[41] G. H. Hines, M. Arcak, and A. K. Packard, "Equilibrium-independent passivity: A new definition and numerical certification," *Automatica*, vol. 47, no. 9, pp. 1949–1956, Sep. 2011.

[42] C. De Persis and N. Monshizadeh, "A feedback control algorithm to steer networks to a Cournot–Nash equilibrium," *IEEE Trans. Control Netw. Syst.*, vol. 6, no. 4, pp. 1486–1497, Dec. 2019.

[43] M. Ye and G. Hu, "Game design and analysis for price-based demand response: An aggregate game approach," *IEEE Trans. Cybern.*, vol. 47, no. 3, pp. 720–730, Mar. 2017.

[44] Z. Liu, Q. Wu, S. Huang, L. Wang, M. Shahidehpour, and Y. Xue, "Optimal day-ahead charging scheduling of electric vehicles through an aggregative game model," *IEEE Trans. Smart Grid*, vol. 9, no. 5, pp. 5173–5184, Sep. 2018.

[45] X. Chen, M. Shakarami, J. M. A. Scherpen, and N. Monshizadeh, "Aggregating distributed energy resources for grid flexibility services: A distributed game theoretic approach," *Int. J. Robust Nonlinear Control*, Jun. 2023.

[46] G. I. Bischi, F. Lamantia, and D. Radi, "An evolutionary cournot model with limited market knowledge," *J. Econ. Behav. Org.*, vol. 116, pp. 219–238, Aug. 2015.

[47] C. Cenedese, G. Belgioioso, Y. Kawano, S. Grammatico, and M. Cao, "Asynchronous and time-varying proximal type dynamics in multiagent network games," *IEEE Trans. Autom. Control*, vol. 66, no. 6, pp. 2861–2867, Jun. 2021.

[48] S. Boyd and L. Vandenberghe, *Convex Optimization*. Cambridge, U.K.: Cambridge Univ. Press, 2004.

[49] K. Nabetani, P. Tseng, and M. Fukushima, "Parametrized variational inequality approaches to generalized Nash equilibrium problems with shared constraints," *Comput. Optim. Appl.*, vol. 48, no. 3, pp. 423–452, Apr. 2011.

[50] P. Yi and L. Pavel, "An operator splitting approach for distributed generalized Nash equilibria computation," *Automatica*, vol. 102, pp. 111–121, Apr. 2019.

[51] A. Nagurney and D. Zhang, *Projected Dynamical Systems and Variational Inequalities With Applications*, vol. 2. Berlin, Germany: Springer, 1995.

[52] Y. Lou, Y. Hong, and S. Wang, "Distributed continuous-time approximate projection protocols for shortest distance optimization problems," *Automatica*, vol. 69, pp. 289–297, Jul. 2016.

[53] Y. Zhao, X. He, T. Huang, J. Huang, and P. Li, "A smoothing neural network for minimization l1-lp in sparse signal reconstruction with measurement noises," *Neural Netw.*, vol. 122, pp. 40–53, Feb. 2020.

[54] H. K. Khalil, *Nonlinear Systems*. Upper Saddle River, NJ, USA: Prentice-Hall, 2002.

[55] W. Schulz, "ETSI standards and guides for efficient powering of telecommunication and datacom," in *Proc. 29th Int. Telecommun. Energy Conf.*, 2007, pp. 168–173.

[56] Z. Fu. (2023). *Case Study: 16 DGUs microgrid*. [Online]. Available: https://github.com/Zao-Fu/DC-micro-grid

[57] P. Yi, Y. Hong, and F. Liu, "Distributed gradient algorithm for constrained optimization with application to load sharing in power systems," *Syst. Control Lett.*, vol. 83, pp. 45–52, Sep. 2015.

[58] K. C. Kosaraju, V. Chinde, R. Pasumarthy, A. Kelkar, and N. M. Singh, "Stability analysis of constrained optimization dynamics via passivity techniques," *IEEE Control Syst. Lett.*, vol. 2, no. 1, pp. 91–96, Jan. 2018.

[59] G. Belgioioso, D. Liao-McPherson, M. H. de Badyn, S. Bolognani, J. Lygeros, and F. Dörfler, "Sampled-data online feedback equilibrium seeking: Stability and tracking," in *Proc. 60th IEEE Conf. Decis. Control (CDC)*, Dec. 2021, pp. 2702–2708.

[60] H. H. Bauschke and P. L. Combettes, *Convex Analysis and Monotone Operator Theory in Hilbert Spaces*, vol. 408. Berlin, Germany: Springer, 2011.

[61] R. T. Rockafellar, *Convex Analysis*. Princeton, NJ, USA: Princeton Univ. Press, 2015.

Zao Fu received the B.S. degree in communication engineering from Jiangxi Normal University, Nanchang, China, in 2014, and the M.S. degree in electronics and communications engineering from Southwest University, Chongqing, China, in 2017. He is currently pursuing the Ph.D. degree with Southeast University, Nanjing, China, and the University of Groningen (UG), Groningen, The Netherlands.

He has held several visiting positions in Canada, Australia, Italy, and The Netherlands. His current research interests include smart grids, distributed optimization and control, and game theory.

Carlo Cenedese (Member, IEEE) received the bachelor's degree in information engineering and the master's degree in control system from the University of Padova, Padua, Italy, in 2013 and 2016, respectively, and the Ph.D. degree in automatic control from the University of Groningen, Groningen, The Netherlands, in 2021.

Since 2021, he has been a Postdoctoral Researcher at the Automatic Control Laboratory (IfA), ETH Zürich, Zürich, Switzerland, where he has also been a Senior Scientist since 2024. His research interests include the design of optimization and game-theoretic algorithms, and the modeling of multiagent systems with applications to traffic control and energy markets.

Michele Cucuzzella (Member, IEEE) received the M.Sc. degree (Hons.) in electrical engineering and the Ph.D. degree in systems and control from the University of Pavia, Pavia, Italy, in 2014 and 2018, respectively.

From 2017 to 2020, he held a postdoctoral position at the University of Groningen (UG), Groningen, The Netherlands. He then joined the University of Pavia as an Assistant Professor. In 2024, he moved to UG as an Associate Professor at the Engineering and Technology institute Groningen, Faculty of Science and Engineering. He is also a Visiting Associate Professor at Hiroshima University, Higashihiroshima, Japan. He has coauthored the book *Advanced and Optimization Based Sliding Mode Control: Theory and Applications* (SIAM, 2019). His research activities are mainly in the area of nonlinear control with application to the energy domain and smart complex systems.

Dr. Cucuzzella is a member of the EUCA Conference Editorial Board and the IEEE CSS Technology Conferences Editorial Board. He received the Certificate of Outstanding Service as a Reviewer of the IEEE CONTROL SYSTEMS LETTERS 2019. He also received the 2020 IEEE TRANSACTIONS ON CONTROL SYSTEMS TECHNOLOGY Outstanding Paper Award, the IEEE Italy Section Award for the best Ph.D. thesis on new technological challenges in energy and industry, and the SIDRA Award for the best Ph.D. thesis in the field of systems and control engineering. He was also the finalist for the EECI Award for the best Ph.D. thesis in Europe in the field of control for complex and heterogeneous systems and the IEEE-CSS Italy Best Young Paper Award. He has been serving as an Associate Editor for the *European Journal of Control* since 2022.

Wenwu Yu (Senior Member, IEEE) received the B.Sc. degree in information and computing science and the M.Sc. degree in applied mathematics from the Department of Mathematics, Southeast University, Nanjing, China, in 2004 and 2007, respectively, and the Ph.D. degree from the Department of Electronic Engineering, City University of Hong Kong, Hong Kong, China, in 2010.

He has held several visiting positions in Australia, China, Germany, Italy, The Netherlands, and USA. He is currently the Dean of the School of Mathematics, the Deputy Associate Director of the National Center of Applied Mathematics, the Deputy Director of Jiangsu Provincial Scientific Research Center of Applied Mathematics, the Deputy Associate Director of Jiangsu Provincial Key Laboratory of Networked Collective Intelligence, and a Full Professor with the Endowed Chair Honor at Southeast University. He has authored about 100 IEEE TRANSACTIONS journal articles with more than 20 000 citations. His research interests include multiagent systems, complex networks and systems, disturbance control, distributed optimization, machine learning, game theory, cyberspace security, smart grids, intelligent transportation systems, and big data analysis.

Dr. Yu was a recipient of the Second Prize of State Natural Science Award of China in 2016. He is also the Cheung Kong Scholars Programmer of the Ministry of Education of China (Artificial Intelligence). He severs as an Editorial Board Member for several flag journals, including IEEE TRANSACTIONS ON CIRCUITS AND SYSTEMS II, IEEE TRANSACTIONS ON INDUSTRIAL INFORMATICS, IEEE TRANSACTIONS ON SYSTEMS, MAN, AND CYBERNETICS: SYSTEMS, IEEE TRANSACTIONS ON INDUSTRIAL CYBER-PHYSICAL SYSTEMS, *Science China Information Sciences*, and *Science China Technological Sciences*. He was listed by Clarivate Analytics/Thomson Reuters Highly Cited Researchers in Engineering from 2014 to 2023.

Jacquelien M. A. Scherpen (Fellow, IEEE) received the M.Sc. and Ph.D. degrees from the University of Twente, Enschede, The Netherlands, in 1990 and 1994, respectively.

She then joined Delft University of Technology, Delft, The Netherlands, and moved to the Engineering and Technology institute Groningen (ENTEG), Faculty of Science and Engineering, University of Groningen (UG), Groningen, The Netherlands, in 2006. She was the Scientific Director of ENTEG and the Director of Engineering at UG, where she is currently the Rector Magnificus. She has been the Captain of Science of the Dutch top sector High Tech Systems and Materials (HTSM). She has held various visiting research positions at The University of Tokyo, Tokyo, Japan; Kyoto University, Kyoto, Japan; Old Dominion University, Norfolk, VA, USA; Université de Compiegne, Compiégne, France; and Supélec, Gif-sur-Yvette, France. Her current research interests include model reduction methods for networks, nonlinear model reduction methods, nonlinear control methods, and modeling and control of physical systems with applications to electrical circuits, electromechanical systems, mechanical systems, smart energy networks, and distributed optimal control for smart grids.

Dr. Scherpen received the 2017–2020 Automatica Best Paper Prize. In 2019, she received a royal distinction as Knight in the Order of the Netherlands Lion. In 2023, she received the Prince Friso Prize for Engineer of the Year in The Netherlands. She has been active at the International Federation of Automatic Control (IFAC) and the IEEE Control Systems Society. She was the President of the European Control Association (EUCA) and has chaired the SIAM Activity Group on Control and Systems Theory. She has been at the editorial board of a few international journals, among which are the IEEE TRANSACTIONS ON AUTOMATIC CONTROL and the *International Journal of Robust and Nonlinear Control*.

Open Access funding provided by ‘Università degli Studi di Pavia’ within the CRUI CARE Agreement